Journal of Building Engineering 97 (2024) 110800

Contents lists available at ScienceDirect

Journal of Building Engineering

journal homepage: www.elsevier.com/locate/jobe

Radiation-shielding concrete: A review of materials, performance, and the impact of radiation on concrete properties

Ali M. Onaizi [a], Mugahed Amran [b,c], Waiching Tang [a,*], Nour Betoush [d], Mohammad Alhassan [d,e], Raizal S.M. Rashid [f], Mohammad Fares Yasin [a], K.H. Bayagoob [g], Sagheer A. Onaizi [h,i]

[a] School of Architecture and Built Environment, The University of Newcastle, University Drive, Callaghan, NSW, 2308, Australia
[b] Department of Civil Engineering, College of Engineering, Prince Sattam Bin Abdulaziz University, 11942, Alkharj, Saudi Arabia
[c] Department of Civil Engineering, Faculty of Engineering and IT, Amran University, 9677, Amran, Yemen
[d] Department of Civil Engineering, Jordan University of Science and Technology, Irbid, Jordan
[e] Civil Engineering Program, Al Ain University, Al Ain, United Arab Emirates
[f] Department of Civil Engineering, Faculty of Engineering, Universiti Putra Malaysia, 43400, Serdang, Selangor, Malaysia
[g] Department of Civil Engineering, College of Engineering, University of Bisha, P.O Box 61922, Bisha, Saudi Arabia
[h] Department of Chemical Engineering, King Fahd University of Petroleum and Minerals, Dhahran, 31261, Saudi Arabia
[i] Interdisciplinary Research Center for Hydrogen Technologies and CarbonManagement, King Fahd University of Petroleum and Minerals, Dhahran, 31216, Saudi Arabia

ARTICLE INFO

Keywords:
Concrete materials
Radiation-shielding concrete (RSC)
Radiation attenuation
Irradiation concrete
Radiation measurement

ABSTRACT

The efficiency of radiation shielding is crucial across industries having radioactive activities, from medical facilities to nuclear power stations. Radiation-Shielding Concrete (RSC) emerges as the preferred material for its cost-effectiveness, robust mechanical performance, ease of production, and excellent radiation attenuation properties against ionizing radiations such as gamma rays, X-rays, and neutrons. This comprehensive review delves into the evolution of SCI indexed research on concrete materials for radiation protection, focusing primarily on studies published in the last decade. It meticulously analyze the latest literature to understand how RSC materials enhance radiation attenuation. The review provides valuable insights into the influence of irradiation on both macro- and micro-properties, enriching the knowledge base for material efficiency and effectiveness concerning different types of radiation and shielding requirements. Additionally, this review with a set of recommendations for future research to advance progress in modern construction, encouraging further examination and innovation in the selection of RSC materials.

List of Abbreviation

RC	The reinforced concrete
RSC	Radiation-Shielding Concrete
UHPC	Ultra-high-strength concrete
HPFRCC	High-performance fiber-reinforced cementitious composites
OPC	Ordinary Portland Cement
EAF	Electric Arc Furnace

(*continued on next page*)

* Corresponding author.
E-mail address: patrick.tang@newcastle.edu.au (W. Tang).

https://doi.org/10.1016/j.jobe.2024.110800
Received 14 June 2024; Received in revised form 11 September 2024; Accepted 18 September 2024
Available online 20 September 2024

(*continued*)

LS	Lead slag
CS	Copper slag
SS	Steel slag
NF	Fe_2O_3-nanoparticles
NZ	ZnO-nanoparticles
GGBS	Ground Granulated Blast-furnace Slag
SA	Siderurgical aggregate
SAC	Siderurgical aggregate concrete
B4C	Boron Carbide
BSGP	Borosilicate glass powder
NPs	Nanoparticle
CNTs	Carbon nanotubes
SEM	Scanning electron microscopy
ASR	Alkali-silica reaction
γ	Gamma ray
HVL	The half-value layer
LAC	The linear attenuation coefficient
MAC	The Mass Attenuation Coefficien
TVL	The Tenth Value Layer
EM	Electromagnetic wave
NDT	Non-destructive testing
ECT	Electrical capacitance tomography
HPGe	High-Purity Germanium
NaI(Tl)	Thallium-doped sodium iodide Scintillation Detectors
NaI	Sodium Iodide Scintillation Detectors
Co60	Cobalt-60
Ba133	Barium-133,
Cs137	Caesium-137

1. Introduction

Despite the shift toward renewable energy, nuclear power remains a vital part of total energy generation globally [1], contributing around 12 % of the world's electricity and are still constantly increasing as shown in Fig. 1 [2]. This is highlighted by the fact that 30 countries operate 439 nuclear reactors, with an additional 64 units currently in the planning stage [2]. Nuclear power constitutes a significant portion of Europe's electrical supply, accounting for more than one-quarter of its total generation; over 30 % of the region's electricity demand is met through nuclear energy, while fossil fuels provide 40 %, and renewables make up the remaining share [3]. As of 2024, Europe has a total of 131 operational nuclear power reactors, and currently, three European Union member states are engaged in the construction of further nuclear power plants [3]. A nuclear facility is essentially a thermal power station that uses a nuclear reactor as its primary heat source [4], and heat is utilized to generate steam, driving a steam turbine connected to an electricity-generating generator [5]. This principle is applied in nuclear power plants to ensure that they fall within the list of clean energy sources, as they do not generate any carbon emissions; this approach enhances efforts to reduce and avoid CO_2 emissions, as

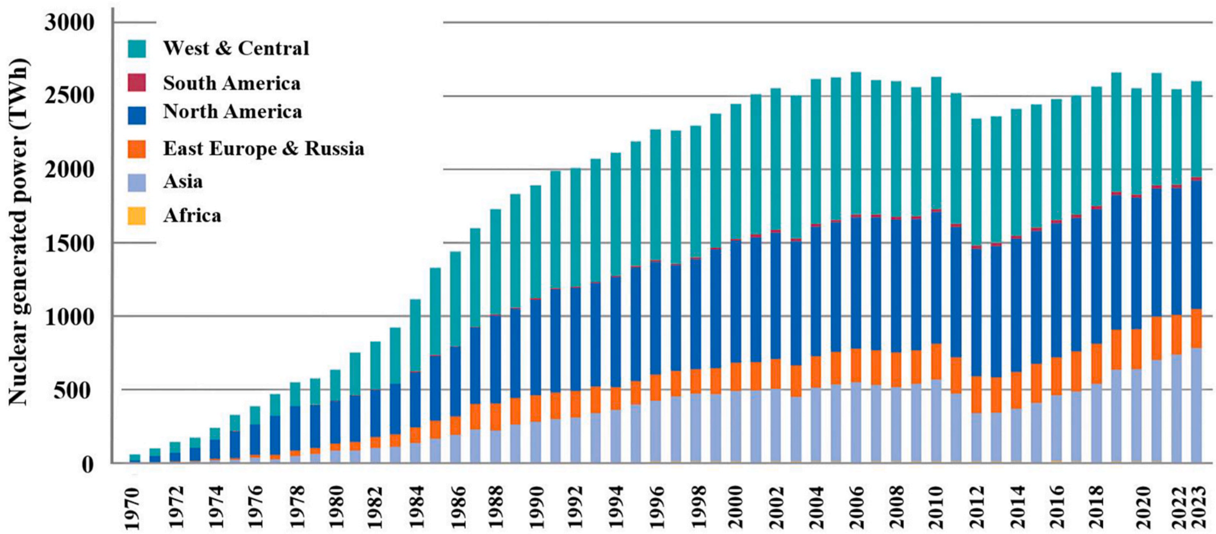

Fig. 1. Nuclear electricity production by region (1970–2023) (adapted from Ref. [17]).

depicted in Fig. 2 [6]. The first nuclear power reactor was established in the United States on December 20, 1951 [7], and interest in building and constructing nuclear fission reactors for energy production for nonmilitary applications peaked in the discourse during the 1970s and 1980s [8]. Owing to the inherent radioactivity of nuclear fission, encasing the reactor core within a safeguarding shell is critical [9], serving as a containment mechanism that effectively mitigates the dispersion of radiation and prevents the release of radioactive substances into the environment [10].

Radiation-shielding concrete (RSC) plays a vital role in protecting against harmful ionizing radiation across various applications [11,12]. In nuclear power plants, it is crucial for safeguarding workers and the environment, forming an integral part of reactor containment structures, spent fuel storage, and waste disposal facilities. Medical facilities also utilize RSC to build walls, floors, and ceilings in diagnostic imaging and radiation therapy rooms, ensuring a safe environment for patients, staff, and visitors [13]. It is also essential in industrial radiography facilities, enabling safe non-destructive testing in aerospace, automotive, and construction sectors [14,15]. Research laboratories that handle radioactive materials depend on RSC for protection and adherence to safety regulations. The military uses it in bunkers and command centers to protect personnel and equipment from nuclear threats. In nuclear waste storage, RSC isolates radioactive materials, preventing radiation from leaking into the environment [16]. Furthermore, in radiopharmaceutical production, it safeguards workers during the production and handling of medical isotopes. Overall, radiation-shielding concrete is indispensable for ensuring safety and regulatory compliance, supporting the beneficial use of radiation in various fields.

The investigation of construction materials for nuclear facilities holds significant importance for the advancement of concrete and consequently enhances human safety. The present review aims to address the existing gap in the literature concerning the comprehensive synthesis and analysis of emerging materials, including high-density aggregates, innovative composites and nanomaterials which have the potential to enhance the radiation shielding properties of RSCs. Radiological protection and shielding represent vital aspects across various industries, spanning from medical facilities to nuclear energy production. This comprehensive review endeavors to explore the dynamic landscape of technological advancements within concrete-based radiation shielding. By conducting an extensive analysis of contemporary literature, this review elucidates the latest trends, innovations, and methodologies employed for augmenting the radiation attenuation capabilities of concrete materials. Through a meticulous synthesis of research findings, this manuscript provides valuable insights into the evolving strategies that contribute to optimizing concrete shielding capabilities. It serves as a valuable resource for practitioners, policymakers, and researchers involved in radiation safety and shielding applications, offering a forward-looking perspective on the future directions of this pivotal field. Moreover, this review aims to provide comprehensive resources that can stimulate further exploration, innovation, and collaboration in the realm of RSC technology within modern construction industries.

2. Radiation shielding fundamentals

The increased utilization of ionizing radiation in various industries has led to significant interest in radiation protection [18]. Radiological protection involves strategies to protect people from the harmful effects of ionizing radiation exposure [19]. The three fundamental principles of radiation protection include time, distance, and shielding, as depicted in Fig. 3 [20]. The effectiveness of radiation shielding depends on factors such as the radiation intensity, the density of the shielding material, and the atomic number of the elements in the shield. Other important aspects of radiation shields include mechanical strength, cost-effectiveness, and resistance to radiation damage [21]. The function of shielding is attenuating radiation, where the attenuation of radiation is proportional to the shield density and inversely related to the radiation energy, meaning that higher energy radiation results in less attenuation. In contrast, the density of the radiation shield and the atomic number of its elements enhance attenuation [18]. The probability of γ-rays interacting with a shield depends on the photon's energy, the atomic number of the shielding material, and its density (ρ) [18].

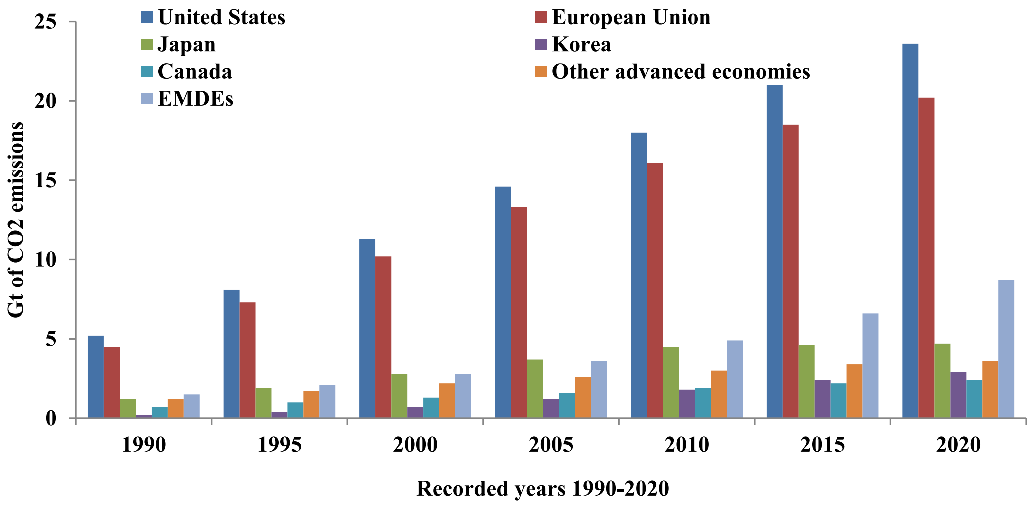

Fig. 2. Cumulative CO_2 emissions avoided by nuclear power by country (Raw data adapted from Ref. [6]).

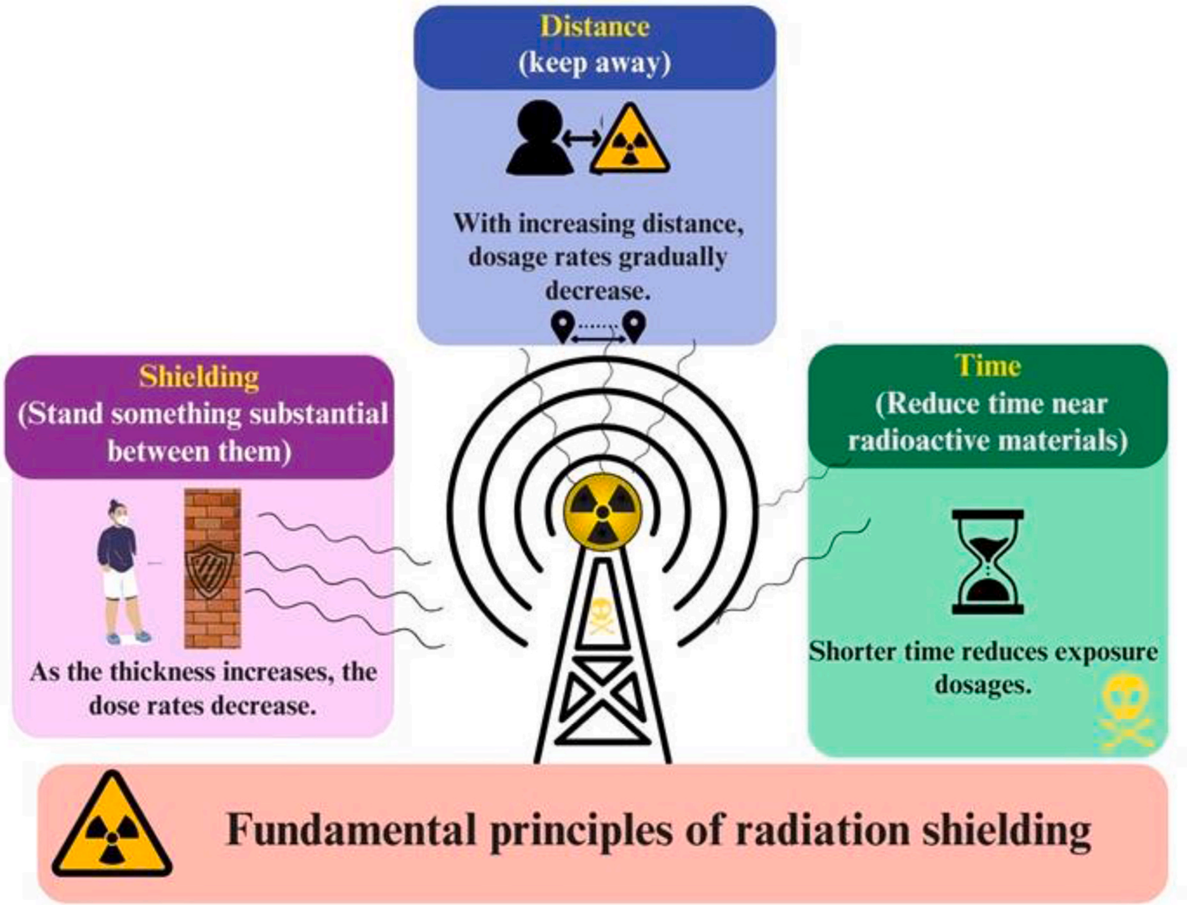

Fig. 3. Basic concepts of radiation shielding.

The mechanism for protecting materials from high-energy electromagnetic gamma rays is relatively simple, whereas shielding against neutrons is more complex [22]. Gamma ray attenuation involves the photoelectric effect, Compton scattering, and pair production. In the photoelectric effect, gamma rays transfer energy to an electron, ejecting it from the atom, which is effective in high atomic number materials [23]. Compton scattering, at intermediate energies, involves gamma rays colliding with electrons and losing energy. Pair production, at high energies, converts gamma rays into electron-positron pairs near a nucleus [23]. High-density materials like lead, Tungsten and Iron, with high atomic numbers, are effective at reducing gamma ray intensity through these mechanisms. Neutrons, which lack charge, interact only with the nuclei of target atoms. The most effective way to attenuate neutrons is through collisions with nuclei of low atomic number elements, such as hydrogen and boron [24–26].

In radiography, the concept of the half-value layer (HVL) is commonly used due to its simplicity in remembering values and conducting straightforward calculations. The HVL refers to the thickness of a material needed to decrease the intensity of gamma radiation by 50 %. This value is typically measured in centimeters (cm). The HVL can be calculated as shown in Eq. (1).

$$HVL = \frac{In\,2}{\mu} \tag{1}$$

Where μ refers to the linear attenuation coefficient (cm^{-1}), and is calculated using the Beer-Lambert formula, as shown in Eq (2) [95].

$$\mu = \frac{1}{d} In\ \frac{T_0}{T} \tag{2}$$

Where T_0 and T are the number of photons the monitoring system collects with and without the RSC material.

Within the context of shielding calculations, having knowledge of the thickness of one HVL enables a rapid assessment of the amount of material required to reduce radiation intensity. The underlying idea in this context is that the efficiency of shielding improves as the thickness of the material increases, in accordance with an exponential correlation [27]. Nevertheless, the impact gradually decreases when more layers of shielding material are incorporated. Another important factor is the Tenth Value Layer (TVL), which represents the thickness of a shielding material required to reduce the radiation intensity to one-tenth of its original value. The

TVL is also measured in centimeters (cm). The calculation of TVL can be represented by the following equation, denoted as Eq. (3).

$$TVL = \frac{In\,10}{\mu} \tag{3}$$

Another parameter is macroscopic removal cross-section, often denoted as Σ_R, is a crucial parameter in the attenuation of radiation, particularly for neutrons. It quantifies the probability of neutron removal per unit path length in a material, taking into account all possible interactions that result in the neutron being effectively removed from the beam. These interactions include scattering, absorption, and any reactions that alter the neutron's energy or direction significantly enough that it no longer contributes to the original beam. It can be determined through Eq. (4), as following [28]:

$$I = I_0 e^{\sum R(E_n)}/x \tag{4}$$

Where I_0 is the total intensity of fast neutron flux emitted from the source within the energy range of 0.8–11 MeV, I is the total intensity of fast neutron flux transmitted from concrete samples within the same energy, E_n is the neutron attenuation coefficient, and x is the definite thickness of the concrete sample within which the flux is transmitted.

Fig. 4 depicts the test setup with reactor neutron flux for neutron shielding evaluation of concrete, while Table 1 presents further information about the radiation sources, detector types and testing setups.

This procedure entails the measurement of neutron transmission through a target material with predetermined thicknesses. To assess the effectiveness of radiation shielding in various concrete mixtures, the thickness of the samples is modified by assembling slabs of the desired thickness. This method enables a meticulous assessment of the recital of different concrete compositions in respect to radiation shielding.

3. Radiation shielding materials

Radiation shields play a crucial role in diverse occupational settings, particularly for individuals working in nuclear energy facilities and for structures specifically engineered to store nuclear waste [52]. The efficacy of radiation shielding is contingent upon the utilization of suitable materials in radiation shielding components [53]. A variety of materials are employed for radiation shielding, including heavyweight concrete, iron, lead, and water, each with distinct features. For instance, while lead is considered optimal for its exceptional shielding capabilities, it is costly and poses significant health risks [54,55]. These components must fulfill health protection standards for individuals who are consistently exposed to radiation, as well as in situations involving unforeseen incidents [56]. Moreover, they are required to adhere to the criteria for the ultimate limit requirements and serviceability, meeting necessary standards for sound and thermal insulation, toughness, and durability [57].

Conventional radiation shields are typically constructed from lead [57]. When stacked to the correct thickness, lead sheets are an effective element in the production of radiation-shielding materials [58]. The clothing is usually available in three standard levels of lead equivalency, 0.25 mm, 0.35 mm, and 0.5 mm, offering different levels of protection [59]. However, despite its efficacy as a protective barrier, lead is acknowledged as a cumulative toxicant substance and has been classified as the second most perilous contaminant by the USEPA. This classification is partly attributed to the tendency of these materials to develop thin oxide coatings that readily detach [60]. Lead poisoning caused by shield exposure can result in severe complications such as cognitive impairment, memory loss, hypertension, anemia, renal damage and even death [61].

Various substitutes for lead in shields have been investigated, including metallic alloys [62], metal oxide-doped glass systems [63], and processed nanobased composites [63]. Nevertheless, most of these materials frequently encounter several limitations, such as exorbitant expenses, restricted adaptability, diminished durability, and complex manufacturing processes. Compared with other shielding materials, the superiority of RSC over several shielding materials such as lead, metal and paper are clearly evident [64,65]. This makes it a preferred choice for shielding in many applications, including nuclear power plants, laboratory hot cells, research reactors, and particle accelerators [66]. Fig. 5 demonstrates the varying effectiveness of different materials in blocking radiation, with

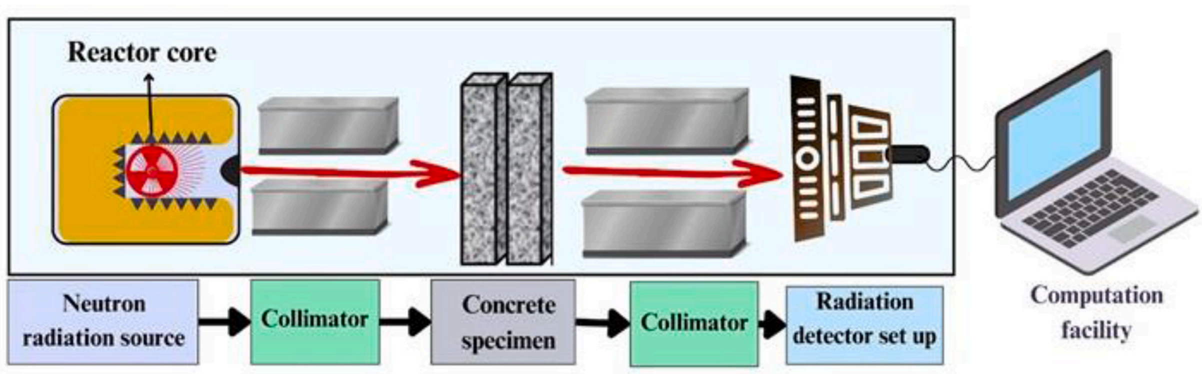

Fig. 4. Test setup with reactor neutron flux for neutron shielding evaluation of concrete (Adopted with improvement from Ref. [29]).

Table 1
Summary of major findings of radiation tests as reported by previous researchers (data collected from Refs. [18,30–51]).

Radiation source	Detector type, mm	Distance from source to specimen (mm)	Duration of count observation, min	Thickness of sample, mm	Distance from detector to specimen (mm)	Dia. of collimator opening, mm	Ref.
Co60	HPGe	790	–	26–182	60	–	[30]
Co60	NaI(Tl)	200	–	20	200	–	[31]
Am241, Co60, Ba133	NaI(Tl)	100			50	Pin hole, (1 cm^2)	[32–34]
Co60, Cs137	–	–	15	20–100	–		[35]
Cs137	NaI(Tl)	330	–	11–16	310	2.8	[36]
Co60, Cs137	Scintillator	20	–	10–40	50	10 slit	[18]
Co60, Cs137	NaI (TL)	50	120	40–120	400	–	[37]
Co60, Cs137	NaI(Tl)	–	–	–	–	18	[38]
Co60, Cs137	NaI(Tl)	–		20–100	–		[39]
Co60, Cs137	NaI(Tl)	20	–	150	50	–	[40]
Cs137	HPGe	100		10–90	100	5	[41]
Co60	HPGe	100		12–36	50		[42]
Cs137, Co60	NaI(Tl)	–	–	100–300	–	8	[43]
Co60, Cs137	NaI(Tl)	147	1.5		286	26	[44]
Cs-137	Berthold LB-6411	300	–	50 to 200	300	3	[45]
Cs137	Scintillation	500	–	–	500	–	[46–48]
Cs137	BaF2 and PSS Scintillators	–	60	80	350	–	[49]
A 150 model, Co60	NaI	200	Long period	100	–	–	[51]
Co60	–	250	< 1 %	100	250	.	[50]

concrete showing the highest efficiency.

4. Radiation shielding concrete

Concrete is a popular choice for radiation shielding due to its affordability, durability, and versatility [65]. The structure and density of RSCs make them effective materials for attenuating γ-rays, especially considering their high density and simple manufacturing process compared to those of pure lead blocks or specialized neutron shielding materials [10,64]. RSC is classified as a safe composite material that consists of cement, water, and heavyweight aggregates [67]. The reinforced concrete (RC) structures proofed that it has the capability to bear various types of loading phenomena, including gravity loads, incidental loads such as impact loads and earthquake forces caused by blast loads, and tornado-generated projectiles, throughout its lifespan [68]. By improving some RC properties to become capable of attenuating radiation, radiation-shielding concrete has become a typical choice for radiation shielding and protection.

Prominent examples of aggregates used in RSC include barite, colemanite, magnetite, and hematite [69–73]. The use of RSC is prevalent in both medical [74] and nuclear applications [75], and its effectiveness is enhanced by the incorporation of dense natural aggregates such as barites, which increase the density of the material to almost 3500 kg/m^3 (a 45 % increase compared to standard concrete), or magnetite, which results in a density of 3900 kg/m^3 (signifying a 60 % increase) [76,77]. Table 2 summarizes the literature findings in terms of influence heavy weight aggregate and alternative materials or additives on strength and shielding properties. Additional merits of RSCs include their superior strength, as depicted in Fig. 6, along with their tailorable properties,

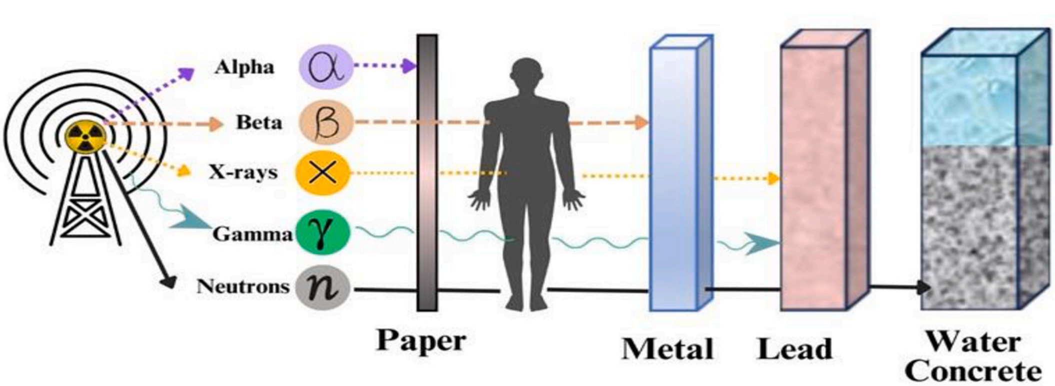

Fig. 5. Types of radiation, penetrations, and properties (Adapted with improvement from Refs. [64,65]).

Table 2
Overview of research on heavy weight and alternative materials used in RSC [51,54,57,78,89–97]

Remarkable constituents		Strength properties	Trend ↑ ↓	Shielding properties	Refs.
Heavyweight aggregates	Magnetite aggregates	Increases in impact resistance by 66 %, ultrasonic pulse velocity by 14 %, and compressive strength by 40 %.	↑	Improvements noted in μ by 8.6 % and the half value layer by 7.9 %.	[92]
	Barite aggregates	Density and tensile strength improved by 17.6 % and 1.2 %, while compressive strength and modulus of elasticity decreased by 3.7 % and 21.12 %.	↑	Improved the attenuation up to 3.1 %	[93]
	Barite aggregates	Improvements in compressive and splitting strengths, and density by 66 %, 101 %, and 138.5 %, respectively.	↑	Attenuation improved by 2.5 %	[90]
	Electric Arc Furnace (EAF) slag aggregate	Density, compressive strength, tensile strength, and modulus of elasticity improved by 17.8 %, 40.64 %, 27.7 % and 34 %.	– ↓	Reduced shielding thickness by 18 % and 19 % compared to ordinary concrete.	[51]
	Combination of basalt, barite and hematite	Basalt with hematite showed the highest compressive strength at 150.6 MPa. Other synthetics also exceeded 140 MPa at 28 days. All synthetics achieved split tensile strengths over 16 MPa with a variation of 0.7 MPa, and flexural strengths above 22 MPa with a variation of 1.5 MPa.	↑	The hematite and barite mix provided the best radiation shielding, with a linear attenuation coefficient of 0.173 cm^{-1}, a half-value layer of 4.01 cm, and a tenth-value layer of 13.28 cm at 1250 KeV.	[98]
	Lead slag (LS), copper slag (CS), and steel slag (SS) as coarse aggregate	The density, compressive strength, tensile strength, flexural strength, and modulus of elasticity ranged from 2605 to 3370 kg/m^3, 92.9–105.8 MPa, 12.1–14.2 MPa, 16.8–19.5 MPa, and 41.97–45.76 GPa, respectively, compared to 2400 kg/m^3, 89.3 MPa, 11.6 MPa, 15.8 MPa, and 40.78 GPa for basalt aggregate. Optimal properties were achieved with 75 % basalt replacement by lead slag.	↑	All radiation attenuation parameters (mfp), linear and mass attenuation coefficients, HVL, and TVL) at 22 °C and 800 °C have been improved. LS, CS, and SS had the highest positive impact on radiation intensities, listed in descending order: 137Cs at 662 keV, 60Co at 1332 keV, and 60Co at 1173 keV.	[99]
Additives and Nanoparticles	Lead-zinc slag wastes	Compressive strength (20 %)	↑	Attenuation improved by 23.1 %	[94]
	Bi_2O_3-loaded concrete	Compressive strength (30 %)	↑	Attenuation improved by 3.15–6.42 %	[95]
	Boron oxide-infused basalt fibers	Enhancement of density in radiation shielding material through basalt-boron fiber integration.	↑	Integration of basalt-boron fibers in concrete shows no impact on gamma-ray shielding, yet markedly boosts neutron shielding, especially in nuclear facilities handling fast or thermal neutron spectra.	[78]
	Furnace steel slag aggregate	Improved compressive strength by 7 %.	↑	Increase the μ and gamma attenuation factor by 14.5 and 5.8 % decrease half value layer by 12.7 %	[97]
	Steel fiber	Density, compressive strength, splitting strength, and flexural strength improved by 2.5 %, 3.3 %, 2.2 % and 0.6 %.	↑	Increased by 10–15 %, depending on the photon energy, compared to conventional concrete	[96]
	Phosphotungstic acid - Copper oxide nanoparticles - Plastic waste nanocomposites	The assembled nanocomposites were found highly protective from γ-rays.	↑	Overall enhancement observed in attenuation characteristics.	[89]
	TiO_2 nanoparticles	By increasing the nano - TiO_2 up to 6 %, the compressive strength is increase by 15.5 %.	↑	By adding 8 % of nano particles the μ for photon energies of 662, 1170, and 1332 keV are increased by 8.9, 5.4, and 7.8, respectively, with respect to those of the reference specimens.	[100]
	Hematite nanoparticles (NF)	The inclusion of 2 % of NF improved compressive strength by around 20 %.	↑	The results reveal that the linear attenuation coefficient values for pastes containing 2 mass % NF increase by 6, 3 and 11 % at 3, 28 and 90 days.	[91]
	ZnO nanoparticles	The incorporation of NZ, up to 0.2 mass %, decreases the compressive strength during all hydration periods.	– ↓	The linear attenuation coefficient value for the paste containing 0.05 mass % NZ (mix Z1) is nearly similar to that of mix B after 3 days of hydration and then decreases by 1.5 and 1.3 % after 28 and 90 days of hydration, respectively	

nonhazardous nature, and feasibility for convenient on-site fabrication [57]. A notable advantage of the RSC is its ability to be mix-designed for effective shielding against both neutrons and gamma radiation [78], a characteristic that is not present in lead. Lead exhibits lower neutron absorption efficiency than does RSC and can produce secondary neutron radiation via photoneutron interactions when used as a shield against high-energy gamma rays with energies above 10 MeV [79,80].

It is known that attenuation efficiency depends on density, rather than compressive strength. Numerous studies have demonstrated a relationship between shielding and density, but the focus on the relationship between shielding and water content has been limited. In this context, Fig. 6 summarizes the results of compressive strength and w/c (water-cement ratio), as it is an indicator of the water content trapped in the pores and the linear attenuation coefficient. As shown in Fig. 6, there is no clear relationship between compressive strength and the linear attenuation coefficient. However, there is a proportional relationship between the linear attenuation coefficient and both of density and w/c, where an increase in w/c with proper density indicates an increase in the linear attenuation coefficient. It is noteworthy that an increase in w/c reduces the density of concrete, but this relationship can be attributed to the effectiveness of the water content in neutron attenuation, as lighter nuclei such as hydrogen are more effective in neutron attenuation compared to nuclei of atoms with larger atomic numbers. Therefore, the capacity of RSC to diminish many forms of radiation, such as alpha rays, beta rays, gamma rays, X-rays, and neutrons, can be linked to its high density and significant concentration of crystalline water [65]. However, concrete has limitations, including its substantial thickness, opacity, tendency to crack under intense radiation, and gradual decrease in density and mechanical strength over time [81].

4.1. Aggregates used in RSC

Several experiments have been carried out to enhance the traditional shielding characteristics of RSC by including various types of aggregates [101]. Heavyweight materials, also known as high-density materials, possess a density greater than that of standard concrete. Normal weight aggregate typically has a density ranging from 2300 to 2500 kg/m^3, whereas heavyweight aggregate exhibits a density exceeding 3000 kg/m^3 according to BS 8110 and EN 206-1 [12,102]. As shown in Table 3, Barite and Magnetite are noted for their high density, which significantly enhances their radiation attenuation capabilities. Barite, with densities ranging from 3000 to 4500 kg/m^3, offers superior radiation attenuation (HVL 3.8–4.0 cm) and moderate compressive strength (20–36 MPa). Magnetite also provides high density (3500–5200 kg/m^3), excellent radiation attenuation (HVL 0.5–2.0 cm), and high compressive strength (20–150 MPa). Siderurgical aggregates, though possessing moderate radiation attenuation (HVL 1.0–3.5 cm) and compressive strength (27–40 MPa), are highly cost-effective and abundantly available.

Boron-containing aggregates exhibit variable densities (1500–2690 kg/m^3) and high boron content (1.0–20.0 %), which is crucial for neutron radiation shielding. However, their thermal conductivity is low (0.5–1.5 W/m·K), and costs can vary significantly. Hematite aggregates stand out with their high density (4000–5300 kg/m^3), moderate radiation attenuation (HVL 0.5–2.5 cm), and high compressive strength (20–150 MPa), making them highly suitable for robust shielding applications. Colemanite, characterized by moderate density (2100–2400 kg/m^3) and high boron content (20.0–60.0 %), is effective for neutron shielding but is limited in availability and has low thermal conductivity (0.5–1.5 W/m·K). Generally, the choice of aggregate is contingent upon specific project requirements, necessitating a balance among factors such as density, radiation attenuation, cost, and availability to achieve optimal performance in radiation shielding concrete. Finally, it is worth noting that there are several potential and sustainable aggregates for use as heavy aggregates to enhance gamma ray attenuation, particularly steel slag [103,104].

4.1.1. Barite aggregates

Barite aggregate, primarily composed of barium sulfate ($BaSO_4$), is valued in construction for its high density, making it an excellent material for radiation shielding in medical and nuclear facilities [123,124]. Its density, typically around 3–4.5 g/cm^3, enhances the attenuation of gamma rays and X-rays [22,65,105–107]. Barite is also chemically inert, non-toxic, and relatively easy to process, ensuring its stability and safety in various applications. It is commonly sourced from barite deposits found in countries such as

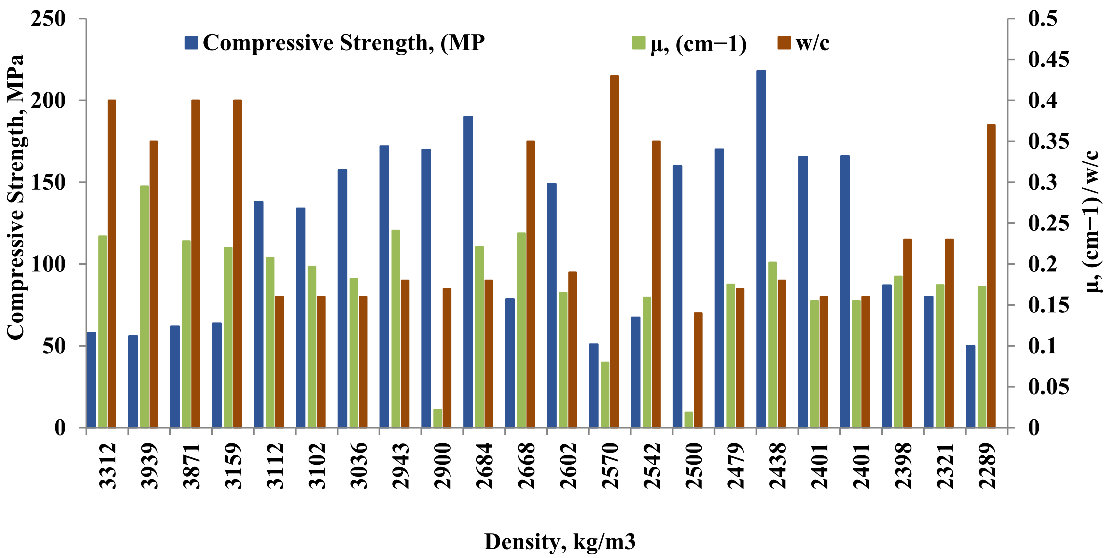

Fig. 6. RSC with high compressive strength (Raw data adapted from Refs. [21,49,65,72,73,82–88]).

Table 3
Detailed comparison of the various aggregates used in the production of RSC.

Property	Barite	Siderurgical	Boron-Containing	Hematite	Magnetite	Colemanite
Density (kg/m^3)	High 3000–4500	High 3590–3760	Variable 1500–2690	High 4000–5300	High 3500–5200	Moderate 2100–2400
Radiation Attenuation (HVL, cm)	High 3.8–4.0	Moderate 1.0–3.5	Variable 0.2–1.0	Moderate 0.5–2.5	High 0.5–2.0	Variable 0.2–1.0
Boron Content, (%)	Low 0.366–0.55	Low 0.01–0.5	High 1.0–20.0	Low 0.01–0.5	Low 0.01–0.5	High 20.0–60.0
Cost	Moderate	Low	Variable	Moderate	Moderate	Moderate
Availability	Abundant	Abundant	Moderate	Abundant	Abundant	Limited
Thermal Conductivity, (W/m·K)	Moderate 1.0–3.0	Moderate 1.0–3.5	Low 0.5–1.5	Moderate 2.0–4.0	Moderate 2.0–4.0	Low 0.5–1.5
Particle Shape	Angular to Subangular	Angular to Subangular	Angular to Rounded	Subangular to Subrounded	Angular to Subangular	Subangular to Subrounded
Compressive Strength, MPa	Moderate 20–36	Moderate 27–40	High 10–100	High 20–150	High 20–150	Moderate 5–50
Workability	Moderate	Moderate	Moderate	Good	Good	Good
Ref.	[22,65,105–107]	[108–110]	[111–115]	[116–118]	[117,119]	[120–122]

China, India, the United States, and Morocco [124–126]. These properties make barite aggregate a practical and effective choice for high-density concrete used in radiation shielding and other specialized construction projects.

Barite concrete exhibits a similar modulus of elasticity and Poisson's ratio as regular concrete, while certain studies have indicated greater modulus of elasticity values for barite concrete than for normal concrete [127]. The use of barite aggregates has been associated with a decrease in compressive strength and an increase in flexural strength [128]. Typically, using barite as a coarse aggregate can increase the normal-weight concrete density to nearly 3500 kg/m^3, while using magnetite can increase it to 5000 kg/m^3 [129]. The increase in density achieved by high-density aggregates significantly enhances the radiation shielding properties of the concrete.

Research has revealed that barite concretes possess advantageous heat insulation properties, primarily due to their lower thermal diffusivity compared to that of normal concretes [130]. Compared with silico-calcareous concrete, barite concrete exhibits superior residual compressive strength at temperatures greater than 500 °C [130]. However, their strength remains much lower than that of granite concrete [131]. An important problem associated with barite concrete is its susceptibility to spalling, namely, explosive spalling, which can occur on the surface of concrete samples when they are heated at low rates of 1 °C/min and 4 °C/min [131,132]. The cracking observed at high temperatures is caused by the low toughness and heat resistance of barite aggregates [67]. Compared with concrete containing barite aggregates, concrete with barite aggregates has demonstrated superior residual mechanical characteristics at 400 °C. SEM images revealed the absence of cracks in samples containing magnetite aggregates at a temperature of 400 °C [132]. These findings indicate that barite aggregates could be a stronger alternative for concrete subjected to moderate temperatures.

In terms of radiation-shielding characteristics, Barite/OPC concrete exhibits the lowest HVL values, namely at 0.66 MeV compared to normal aggregate/GGBS/OPC, gravel/sand/OPC, normal sand/OPC combinations (Table 4). Regarding linear attenuation coefficient (LAC), Barite/OPC exhibits the highest values at 0.66 MeV, suggesting its excellent ability to attenuate radiation in a linear manner. The Mass Attenuation Coefficient (MAC) values provided pertain exclusively to energy levels of 0.66 MeV and 1.33 MeV. Among the tested materials, the composite of coarse barite and fine normal aggregates mixed with OPC exhibited the highest MAC values, while the composite of normal sand and OPC exhibited the lowest MAC values. This suggests that the coarse barite/fine normal aggregates composite is the most efficient in attenuating radiation at these specific energy levels, when considering the mass of the material. It was reported that concrete with 100 % barite aggregate had higher photon radiation shielding [133]. As shown in Fig. 7, the linear attenuation coefficient values of heavyweight concrete including 100 % barite (B100) are about 47 % and 70 % higher than that of concrete including 100 % normal aggregate (N100) at 6 and 18 MV X-rays, respectively.

In summary, the previous research underscores the superior radiation-shielding capabilities of barite/OPC concrete, particularly at

Table 4
Comparison between Barite-based RSC and other aggregate in terms of radiation-shielding characteristics **(data collected from** Refs. [42,134–138]**).**

The energy level of the radiation		Barite/OPC [134]	Barite/OPC [135]	Aggregate/GGBS/OPC [42]	Coarse barite/fine normal aggregates/OPC [136]	Gravel/sand/OPC [137]	Normal sand/OPC [138]
HVL, MeV	**0.66**	2.714	2.316	4.414	2.605	–	–
	1.33		–	–	5.262	–	–
	1.50	–	–	–	–	4.226	–
LAC, MeV	**0.66**	0.255	0.299	0.157	0.266	–	–
	1.33	–	0.168	–	0.132	–	–
	1.50	–	–	–	–	0.164	–
‘ **MAC, MeV**	**0.66**	–	–	0.084	–	–	0.078
	1.33	–	–	–	–	–	0.055
	1.50	–	–	–	–	0.071	–

lower gamma-ray energy levels, due to its high linear and mass attenuation coefficients. However, the practical application of barite is challenged by its fragility and propensity to produce dust, which requires meticulous handling during the mixing process to maintain the integrity of the concrete composite.

4.1.2. Siderurgical aggregate

The incorporation of electric arc furnace (EAF) slag, a type of siderurgical aggregate (SA), into recycled concrete [264] and high-performance self-compacting concrete (HPSCC) represents a promising yet underexplored avenue in the field of RSC [139,140]. While the use of SA in RSC is gaining traction, existing research predominantly focuses on its behavior under gamma radiation, particularly from cesium-137 sources [141]. This narrow focus reveals a significant gap in the literature, as the response of SA-incorporated concrete to other forms of radiation, such as neutron exposure, remains inadequately understood [142].

The feasibility of using SA in concrete has been validated from both environmental and economic perspectives, yet the implications for radiation shielding, especially in diverse radiation environments, require further scrutiny. Extensive research has been conducted on the effects of the water-to-cement ratio on the mechanical properties of concrete, with findings indicating its critical role in determining structural integrity and fracture resistance [143–145]. However, when examining the water-to-cement ratio's influence on radiation attenuation, particularly for cesium-137 and neutrons from an Americium-Beryllium source, the impact appears negligible in limestone-based concrete [146]. This raises questions about the broader applicability of these findings across different concrete compositions and radiation types.

Further studies highlight the importance of the water-to-cement ratio, cement content, and the inclusion of air-entraining agents in moderating gamma radiation, particularly at energies around 384 keV, suggesting that a lower water-to-cement ratio can effectively reduce radiation transmission rates [47,110]. These findings, however, are limited by their focus on gamma radiation, leaving the behavior of such concrete mixtures under neutron radiation less thoroughly investigated. The application of advanced predictive techniques, such as artificial neural networks, to forecast the effectiveness of concrete in shielding thermal neutrons, indicates that optimal shielding performance is achieved with a water-to-cement ratio of 0.38 and a cement content of 400 kg/m^3 when using a Californium-252 source [147]. While these results are promising, they highlight the need for a more comprehensive understanding of how these parameters interact across different types of radiation.

In terms of density impact, the ratio of transmitted to incident intensity is often represented as a function of mass thickness. Fig. 8 shows the mass thickness and neutron attenuation relationship for concretes with various type of aggregates, where the mixture consisting of siderurgical aggregate concrete (SAC) shows better attenuation performance than the mixture consisting of magnetite aggregate (MMC) [109]. This similarity is attributed to the balance between the high iron content and the density of magnetite aggregates. It can be concluded that while concrete containing siderurgical aggregates offers moderate radiation shielding capabilities, its effectiveness varies depending on the composition of the aggregate. Specifically, aggregates with a higher proportion of lighter elements demonstrate improved neutron attenuation, whereas those rich in heavy atoms tend to be less efficient in this regard, but more efficient gamma-ray attenuation. This highlights the importance of carefully selecting the aggregate composition to optimize the shielding properties of siderurgical concrete.

4.1.3. Boron-containing aggregates

Obtaining and utilizing boron in its elemental form is difficult due to its lack of natural occurrence under pure conditions [148]. As a result, numerous boron compounds, including diverse compositions and particle sizes, have been utilized as replacements for aggregates in concrete mixes [149]. Nevertheless, there are some concerns relating to the negative effects of some boron compounds on hydration characteristics. Specifically, borax and boric acid, which are recognized as boron compounds, impede the solidification process of Portland cement, even when present in modest amounts [26,150]. The presence of various boron compounds, such as colemanite, ulexite, borax, and boron carbide, also has a negative effect on the physical and mechanical characteristics of concrete when they are incorporated as either large or small aggregates or in the form of powder [151].

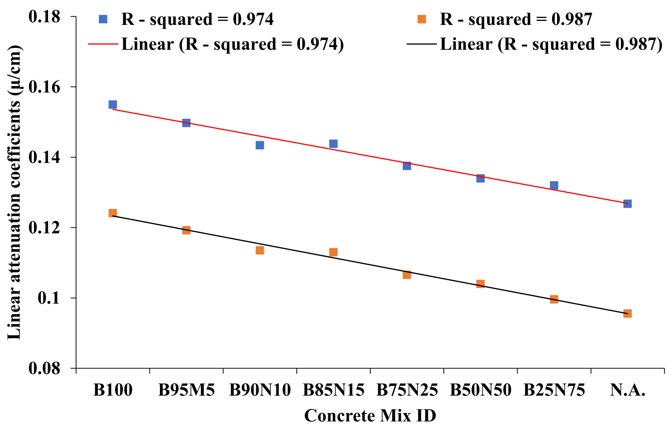

Fig. 7. The µ/cm of mixtures barite aggregate concentration in mixtures with barite for 6 and 18 MV X-rays. The number behind letter B represents barite percentage (Adopted from Ref. [133]).

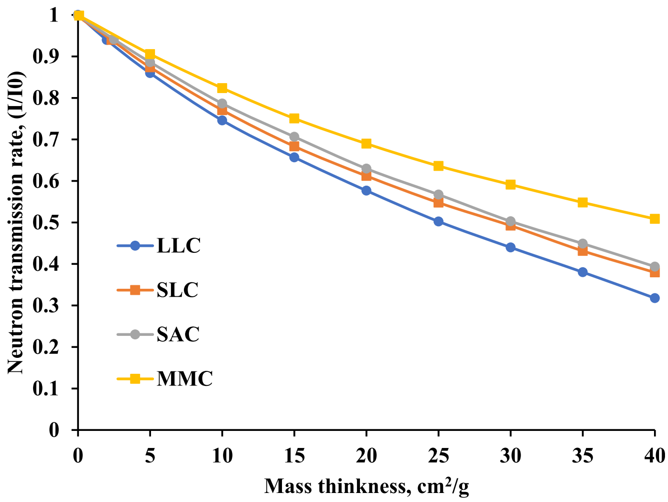

Fig. 8. Rate of neutron transmission with different siderurgical aggregates. (Adapted from Ref. [109]). LLC refers to limestone concrete as coarse and fine aggregate, SLC refers to the concrete with coarse siderurgical aggregate and limestone fine aggregate, SSC refers to concrete mix with siderurgical aggregate as fine and coarse aggregates and MMC refers to concrete mix with fine and coarse fractions of magnetite aggregates.

Isothermal calorimetry was used to study the effects of adding colemanite, ulexite, borax, and synthetic boron carbide as partial sand replacements on the cement hydration kinetics, setting time, and mortar compressive strength at 3 and 28 days [152]. The results verify that ulexite, borax, and colemanite, despite having low levels of boron, have negative impacts on the process of cement hydration and setting time. These effects are shown to be associated with the presence of soluble minerals in the boron aggregates. Nevertheless, mortars containing a maximum of 40 % synthetic Boron Carbide (B4C) powder, with particle sizes ranging from 90 to 125 μm, exhibited no delay in the setting process and a slight increase in the overall heat produced by the cement. The lack of soluble minerals in the synthetic B4C powder, together with the absence of leaching tests or other mineral composition studies, was identified as the cause of this conclusion [153]. The practical implementation of these discoveries may be restricted, given that the majority of high-quality commercially accessible B4C powder comprises a minor proportion of soluble boron. Remarkably, the inclusion of 1–2 % nanosilica, based on the weight of the cement, in colemanite and ulexite greatly accelerated the process of hydration and counteracted the delay induced by soluble boron compounds [1,153]. For neutron shielding, replacing almost 22 % of limestone with boron carbide was found to be sufficient for effective attenuation of polyenergetic neutrons [154].

Borosilicate glass, which consists of more than 80 % silica and can contain up to 15 % boron trioxide, is also renowned for its ability to withstand sudden changes in temperature and is extensively utilized in several industries. The pozzolanic reactivity and neutron shielding capabilities of borosilicate glass powder (BSGP), with an average particle size of 13 μm, were assessed because of its elevated silica and boron content [155]. The maximal pozzolanic reactivity of the BSGP was nearly 55 %, which falls between the normal reactivity of class F fly ash (about 30 %) and that of silica fume (almost 80 %). Several studies revealed that including 25 % BSGP as a substitute for cement led to an 8 % increase in the compressive strength of the mortar. Furthermore, the mortar exhibited a 10–40 % enhancement in neutron attenuation, which was dependent on the degree of BSGP replacement and the duration of curing [153]. Nevertheless, the mortar attenuation coefficient reached a point of stability when 25 % of the BSGP was used as a replacement. This plateau was ascribed to a decrease in hydration and pozzolanic processes [153]. To address the conflicting impacts on the effectiveness of shielding and the qualities of concrete in terms of setting and strength, Yadollahi [147] found that the use of colemanite in concrete mixtures can effectively balance both thermal neutron shielding capabilities and compressive strength. In addition, the use of colemanite ore waste as a cost-effective agent to reduce shrinkage in concrete was demonstrated [156]. Nevertheless, it is crucial to acknowledge that the majority of studies concerning shielding primarily examine the attributes of completely solidified concrete, such as its strength, rather than the initial strength and related qualities of cement solidification.

4.1.4. Hematite aggregates

It has been shown that incorporating hematite into concrete improves its mechanical characteristics at a typical temperature of 25 °C [157]. A.M. Ibrahim et al. [158] found that the incorporation of hematite as a replacement for coarse aggregate in concrete mixtures has resulted in increased hardened concrete density by 3.74 %, 7.70 %, and 11.84 % for replacement ratios of 10 %, 20 %, and 30 %, respectively, compared to the control mixture. The same study [158] demonstrated that replacing coarse aggregate with hematite by 10 %, 20 %, and 30 % increases compressive strength by 16.70 %, 38.55 %, and 41.21 %, respectively, compared to the control mix with CEM III, and by 7.96 %, 18.58 %, and 31 % for concrete with CEM II. This enhancement can be attributed to the rough surface texture of hematite and iron slag, which significantly improves the interfacial zone between the cement paste and coarse aggregate, a critical factor in boosting compressive strength.

Similarly, Beaucour et al. [67], demonstrated that hematite concrete exhibits enhanced compressive, flexural, and tensile strength, along with improved elasticity, following exposure to temperatures between 250 and 400 °C in comparison to traditional silico-calcareous concrete. In contrast, Ibrahim et al. [158], found that replacing normal coarse aggregate with 10 % and 20 % hematite reduces the splitting tensile strength in concrete with CEM II by 14.1 % and 7.5 %, respectively, compared to the control mix. Similarly, for concrete with CEM III, the hematite replacement decreases splitting tensile strength by 8.1 % and 12.67 %, respectively [158]. Similar findings were demonstrated by other studies [31,159].

Another concern when using hematite as a substitute for aggregate is the loss of mass and compressive strength in elevated temperatures behind 400 °C. Fig. 9 shows the TGA/DTA analysis of concrete containing 10 %–40 % of hematite aggregate (H10 - H40). As shown in Fig. 9, the concrete with hematite showed higher loss of mass for compared to the compression sample (H0). Since the hematite in the sample contained calcite ($CaCO_3$), as the replacement ratio increased, the mass loss of the sample also increased. Generally, research on the impact of high temperature on hematite-based concrete is limited. In case of (UHPC), Azreen et al. [73], found that the compressive strength of UHPC containing hematite was less than its counterparts containing silica sand, but it surpassed that of barite. In terms of thermal conductivity, several previous revealed [158,160,161] that the hematite aggregate enhanced the thermal conductivity value in the concrete mixes. This result can be attributed to the high density of hematite compared to normal aggregate, which positively correlates with thermal conductivity.

In terms of radiational shielding properties, the majority of research revealed good improvement with hematite aggregate. For example, compared with ordinary concrete, the μ value of the hematite UHPC (at a 40 % replacement ratio) increased by 43 % and the HVL thickness was reduced by 30 % [162]. Another study [158] found similar result with regular strength concrete, where the replacing aggregate with hematite improved the linear attenuation coefficient by 11.42 % at 661.66 keV compared to the control mix. Similar enhancements were observed at energies 1173.23 keV and 1332.5 keV, with approximately the same percentages of increase. This improvement in shielding properties is likely due to the high density of the aggregates used as a replacement for coarse aggregate, which makes up about 50 % of the concrete volume. Additionally, the atomic number of these aggregates helps to attenuate gamma rays, reducing their penetration in concrete barriers [96,136,163]. Moreover, the HVL and TVL for 60Co and 137Cs for both binder types were reduced by approximately 10.64 % and 8.50 %, respectively, when hematite and iron slag aggregates were used, compared to the control mixture [158]. Fig. 10 illustrates a simulation of UHPC using Monte Carlo software for Dry Cask was performed to study the radiation absorption capability of the mixes. H-UHPC with hematite aggregate) exhibits a higher potential to be used as a gamma-ray shield because of its high density, comparable to that of barite (B-UHPC).

4.1.5. Magnetite aggregate

Magnetite aggregate, composed primarily of iron oxide (Fe_3O_4), is renowned for its high density, which makes it an ideal material for radiation shielding and heavy concrete applications [53]. Tamayo et al. [109] found that magnetite aggregate is 80 % denser than limestone and 20 % denser than siderurgical aggregate. Its magnetic properties and high iron content also contribute to its use in specialized industrial applications. One of its preferable characteristics is its chemical stability which provides excellent durability [164]. It is commonly sourced from mineral deposits in countries such as South Africa, Sweden, Australia, and the United States [165]. These properties make magnetite aggregate a valuable material for constructing radiation-shielding structures, ballast for offshore pipelines, and other high-density concrete projects.

Research has delved into the gamma radiation shielding capabilities of concrete samples containing magnetite and limonite ores [54]. Furthermore, numerous research projects have concentrated on analyzing the radiation protection properties of concrete, investigating how various materials impact the mass attenuation coefficient for gamma rays and the macroscopic effective removal cross-sections for fast neutrons.

[166]. Investigations into the shielding effectiveness of concrete against both neutrons and photons, with varying concentrations of hematite, have revealed that incorporating hematite not only boosts gamma ray attenuation but also strengthens the concrete mechanically, without affecting neutron attenuation [31]. The results obtained for magnetite aggregate concretes showed that linear attenuation coefficients decrease with increasing gamma energy and increase with increasing concrete density. Variation of linear

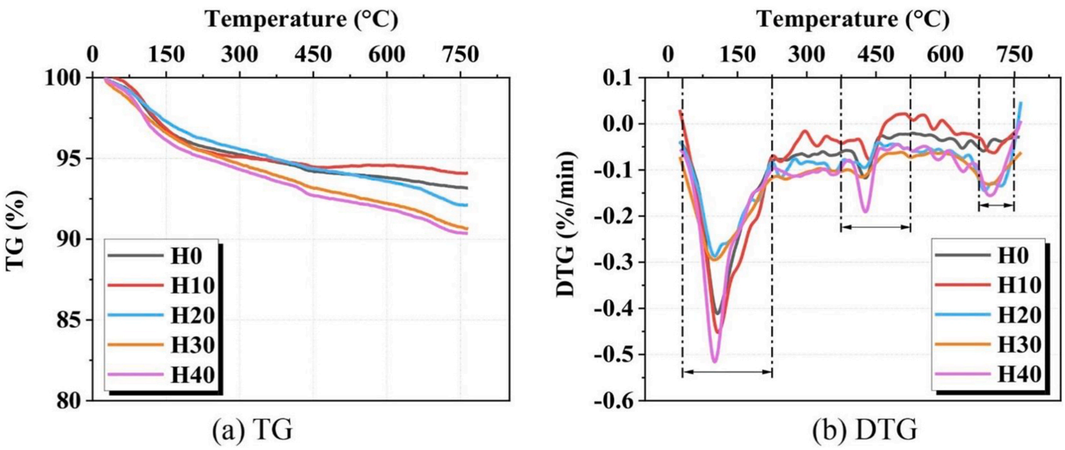

Fig. 9. Thermogravimetric analysis results for the hematite UHPC containing 10 % (H10), 20 % (H20), 30 % (H30) and 40 % (H40) of hematite as aggregate replacements [162].

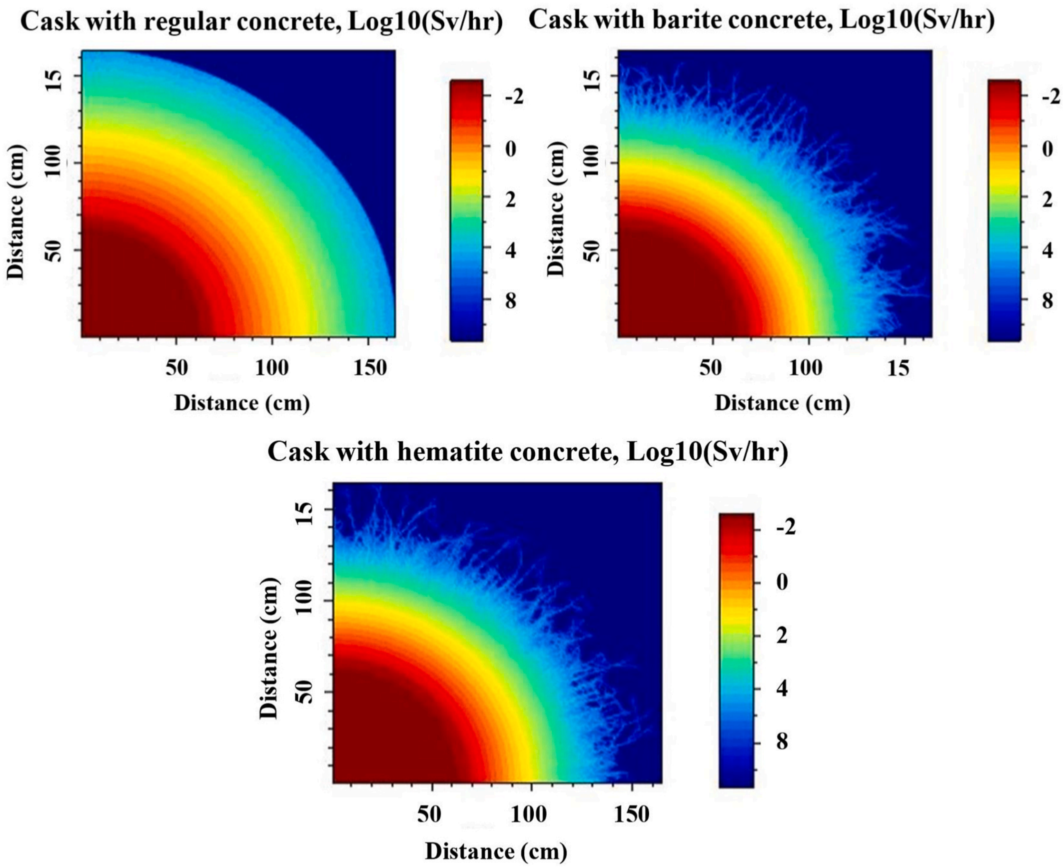

Fig. 10. A 3D simulation of dry cask storage composed of an inner basket with 17 × 17 pressurized water reactors (PWR) fuel assembly, and different concrete shield [73].

attenuation coefficient depending on gamma ray energy and concrete density has been well studied [101,167,168].

4.1.6. Colemanite aggregates

Colemanite is well acknowledged as a prominent candidate for use in diverse applications, principally owing to its ample accessibility and the possible financial advantages of reusing colemanite ore waste from mining locations [169]. Furthermore, it is widely employed in the production of boric acid [170]. As a result, some related research has focused on its use as an aggregate [147]. In the nuclear industry, colemanite is a popular choice for creating radiation-shielding concrete prototypes [171] and has been proven to be effective at reducing radiation transmission [172] and diminishing the medium- and long-term activation of concrete for radiation emission [173]. When combined with high-density aggregates, concrete containing colemanite or other boron minerals has demonstrated low radioactive permeability, effectively blocking both neutron and gamma radiation [32]. These materials have been successfully utilized not only in heavy concrete biological shields for nuclear reactors and research labs [174] but also in neutron therapy centers, including radiation oncology and radiology departments [174]. Furthermore, their exceptional radiation shielding properties have proven to be effective in enhancing protection against Am-Be sources, which release both neutrons and gamma rays [175]. Using colemanite concrete has been shown to be a simpler and more efficient solution than using gamma shields, such as lead blocks, in combination with neutron-absorbing materials such as paraffin. In environments with high-energy gamma- and X-ray sources, the lower atomic number of elements in colemanite concrete offers an advantage over lead shields, particularly in the regions of pair production and Compton scattering [133].

Several studies have investigated the physical and mechanical characteristics of concrete containing different quantities of colemanite [151]. The combination of cement and colemanite waste is highly effective at providing protection against neutrons. A shielding slab has been fabricated with a composite of epoxy resin and colemanite [175]. Furthermore, research had done to study the γ-ray and neutron blocking properties of concretes that include colemanite [176]. Concrete or mortar contains a mixture of many light and heavy elements and therefore has good nuclear properties for the attenuation of photons and neutrons. To shield neutrons, light elements (elements with low atom numbers) are needed. It is common practice to add boron to concrete to try to enhance the thermal neutron attenuation properties and to suppress secondary γ-ray generation.

5. Alternatives and nanomaterials

5.1. Nanomaterials

In recent years, there has been growing interest among researchers in creating a new generation of solid shielding materials enhanced with micro- or nanoparticle (NPs) additives [177,178]. NPs, particularly those smaller than 100 nm, are effective at filling micropores within the RSC matrix, thus improving the strength and durability properties of concrete [57,179]. When present at lower concentrations (up to 10 %), magnetite nanoparticles disperse evenly throughout the cement matrix, thereby strengthening it. This distribution facilitates the process of filling the pores and intensifies the hydration reaction [93]. Nevertheless, when the concentration of these nanoparticles increases, they tend to clump together, resulting in uneven dispersion and the formation of small pores [180]. It has been reported that nanoparticles are effective at decreasing pore sizes, which in turn increases the interaction probability with γ-rays, leading to an improvement in the mass attenuation coefficient [18]. Several of those studies confirmed the relationship between the lime/silica ratio in concrete specimens and gamma radiation absorption, as well as variations in the attenuation coefficient for cement-based composites [181]. A similar study on high-performance concrete revealed the linear relationship between the compressive strength of heavy concrete and γ-ray attenuation [76]. However, no study has specifically focused on the impact of the percentage of added materials on γ-ray attenuation in concrete. Kim et al. [182] also showed that the use of tungsten nanoparticles (nano-W) is more effective than the use of micro-W particles. In a separate study, Tekin et al. conducted a simulation including a composite mixture of micro- and nanosized WO_3 and Bi_2O_3 particles with hematite-serpentine using the MCNPX code [183]. They measured the mass attenuation coefficient across photon energy ranges of 0.142–0.133 MeV and found that the μ/ρ ratios for nanoparticles were greater than those for microparticles at all energy levels (Fig. 11) [183].

In addition, TiO_2, known for its high dielectric loss factor as an n-type semiconductor, is frequently used in composite materials for electromagnetic radiation shielding [184,185]. Spinel ferrites, such as $MnFe_2O_4$, $ZnFe_2O_4$, and $CoFe_2O_4$, are widely used in various applications, including data storage, magnetic resonance imaging, and electronic devices [186]. The magnetic properties of metal oxide nanoparticles are influenced by their size, shape, and morphology [187]. Zinc ferrite, for example, with its significant surface area, is effective as a catalyst in various chemical reactions and is particularly suitable for electromagnetic radiation shielding due to its magnetic and electromagnetic properties, high resistance, high permeability, and chemical stability [188,189].

Carbon nanotubes (CNTs), formed by rolling graphite into cylindrical shapes, are renowned for their exceptional electrical conductivity and effectiveness in shielding against electromagnetic radiation [190,191]. Research has shown that incorporating CNTs into materials can significantly enhance their electromagnetic shielding capabilities, particularly at concentrations up to 2.0 %. For instance, samples with 2.0 % CNTs achieved a shielding effectiveness of 41 dB at a frequency of 3.45 GHz, demonstrating substantial protection within the 4.0 GHz frequency range [192].

Further studies have explored the integration of CNTs into concrete to enhance protection against electromagnetic frequencies, particularly up to 1.12 GHz. When up to 3.0 % CNTs were incorporated into 15 cm thick concrete samples, the shielding capacity improved markedly, with the concrete providing 50 dB of protection at 1.1 GHz, compared to just 10 dB for ordinary concrete [193] This refer to the significant impact of CNT concentration on the electromagnetic shielding performance of concrete. The effectiveness

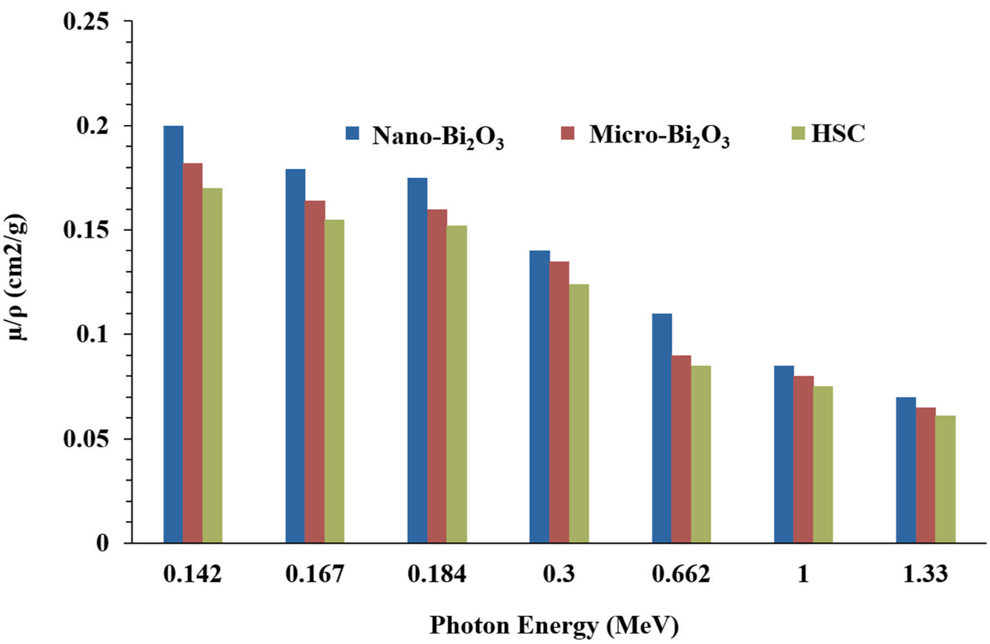

Fig. 11. Comparison of the coefficients of mass attenuation of serpentine-hematite concrete among pure concrete and micro/nano-Bi_2O_3 particles (Adopted from Ref. [183]).

of a 3 cm thick wall made of reinforced concrete combined with a CNT composite was also assessed across a broader frequency range, up to 8 GHz. The findings revealed that increasing the CNT content to 3.0 % enhanced the shielding effectiveness, with the highest electrical conductivity observed at this concentration [194]. Additionally, increasing the thickness of the concrete composite containing 3 % CNTs to 30 cm dramatically improved the shielding efficiency to 80 dB, far surpassing the protection offered by similarly thick concrete without CNTs [195].

Similar improvements were observed when CNTs were integrated into mortar. Studies comparing the electromagnetic shielding capabilities of mortar reinforced with multiwalled carbon nanotubes (MWCNTs) and steel fibers found that CNTs were more effective in enhancing electrical conductivity than steel fibers [196]. Moreover, the impact of adding titanium dioxide and steel fibers to mortar on its ability to reflect electromagnetic radiation up to 18 GHz was also examined. The results indicated that higher concentrations of additives, especially titanium dioxide, significantly improved protection, outperforming the effects of carbon nanoparticles [197]. These findings confirm the potential of CNTs, particularly when used at optimal concentrations and in combination with other materials, to substantially improve the electromagnetic shielding properties of concrete and mortar across various frequency ranges.

5.2. Fibers

Several studies investigated the potential developing of RSC with steel fiber. Fig. 12 summarizes of their findings. As shown in Fig. 12, the optimal LAC range for enhancing compressive strength does not necessarily coincide with the steel fiber content, highlighting the complex interplay between mix components and the resulting mechanical properties of concrete. Chiou et al. [198] investigated the electromagnetic wave (EM) shielding capabilities of concrete by integrating short carbon fibers. Their findings showed a significant improvement in EM reduction, with an increase from 0.5 dB in regular concrete to an astonishing 10.2 dB in EM shielding concrete at a frequency of 1.5 GHz.

Yoo et al. [199], explored the impact of carbon fiber and its surface treatments on the mechanical properties and electromagnetic shielding effectiveness of UHPC. Carbon fibers were treated with sodium hydroxide, nitric acid, and ammonia solutions, and compared to plain carbon fiber at 0.1 and 0.3 wt% contents. The findings showed that nitric acid-treated carbon fibers, which had the highest oxygen content, provided the best tensile performance and energy absorption. Electrical conductivity increased with higher fiber content, and chemically treated fibers showed slightly better conductivity at 0.1 wt%. Both steel and carbon fibers enhanced electromagnetic shielding, with higher carbon fiber content yielding better results. The highest EM shielding effectiveness was 49.0 dB at 1 GHz with 0.1 wt% nitric acid-treated fibers, 23 % higher than plain fibers. Overall, shielding effectiveness increased with conductivity, but the correlation was minor.

Similarly, Park et al. [200] showed that nitric acid-treated fibers provided the best tensile performance and highest shielding effectiveness in high-performance fiber-reinforced cementitious composites (HPFRCC), achieving 49.0 dB at 1 GHz with 0.1 wt% content. The electrical conductivity increased with fiber content, with treated fibers showing slightly better results at lower content. SE was mainly influenced by the amount of carbon fibers, rather than conductivity. HPFRCC with as little as 0.2 vol% carbon fiber achieved high SE (40 dB, 99.99 %) if fibers were well-dispersed, and maintained high compressive strength (101 MPa). Overall, increasing carbon fiber content improved shielding properties, with the highest results achieved by treated fibers. Zorla et al. [78]

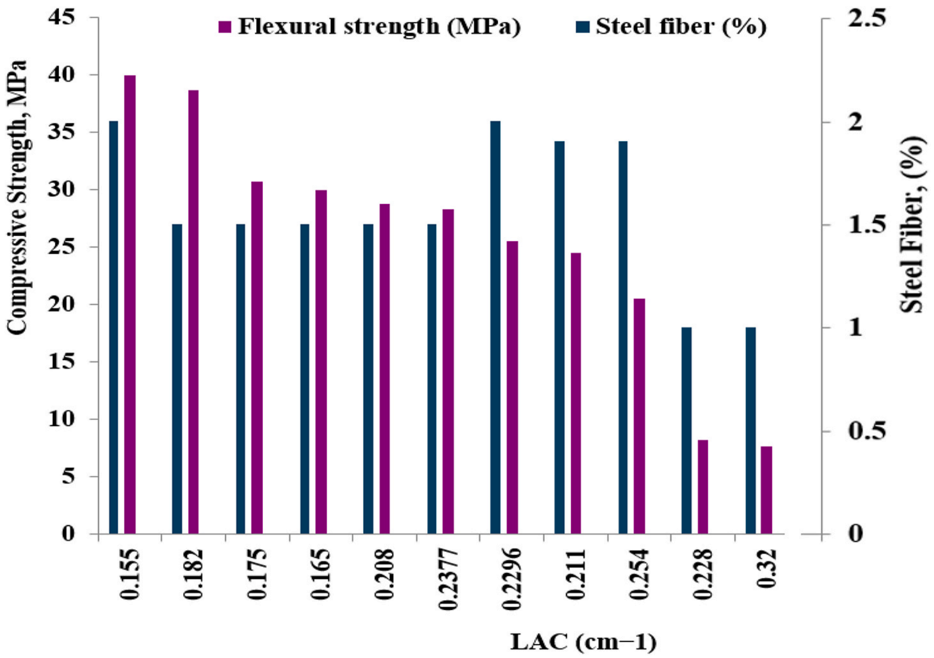

Fig. 12. Impact of steel fiber on the flexural strength and LAC of the RSC (Raw data adapted from [21,65,72,73,83,88].

compared the gamma and neutron attenuation properties of concrete reinforced with basalt fibers infused with natural and enriched boron and barite aggregate. Their findings showed that Gamma-ray attenuation coefficients increased with concrete density but not with the increased content of basalt-boron fiber and the HVL was strongly related to concrete density, with negligible effects from basalt-boron fiber. Concrete with barite aggregate provided better gamma-ray shielding compared to that with basalt fibers due to low concentration. However, basalt-boron fibers significantly improved shielding for fast fission spectrum neutrons.

6. Influence of irradiation on concrete performance

6.1. Mechanical properties

Most studies evaluating the mechanical properties of radiation shielding concrete have primarily focused on the impact of materials used to mitigate radiation on enhancing or reducing mechanical performance. Most published studies compare the effect of various additives on enhancing the concrete's ability to shield against radiation with that of ordinary concrete. However, it is worth noting that relatively few studies have been conducted to assess the impact of irradiation on the mechanical performance or properties of concrete that has already been exposed to radiation. Understanding the effect of radiation on the mechanical properties of concrete is crucial, as radiation exposure can significantly alter the material's performance, potentially compromising its structural integrity over time.

Ichikawa and Koizumi [201], studied the impact of nuclear irradiation, including both neutrons and gamma-rays, on quartz in RSC. The findings reported that crystalline quartz (α-quartz) with a specific gravity of approximately 2.65 transforms into distorted amorphous quartz with a specific gravity of 2.27 when subjected to a fluence of 10^{20} n/cm^2 for fast neutrons with energy levels exceeding 0.1 MeV, as well as under a dose of 10^{12} Gy for beta- and gamma-rays. Maruyama et al. [202] demonstrate that siliceous aggregates undergo expansion as a result of neutron collisions. These collisions deform atomic alignments and leave a portion of the energy from the neutron impacts as strain energy, leading to permanent distortion. Additionally, denser siliceous aggregates are more susceptible to expansion when exposed to neutron irradiation.

The atomic structure of certain aggregates can transform from a crystalline structure to a distorted amorphous structure, resulting in an increase in volume and a decrease in weight. This radiation-induced swelling of aggregates is believed to be directly linked to the degradation of concrete's mechanical properties [203]. The transformation of crystalline quartz into distorted quartz results in two significant negative impacts: (i) microcracking due to differential volume changes within the composite and (ii) increased cracking into the concrete matrix, exposing it to being penetrated by harmful ions [1,204,205]. Both of these effects are harmful to the long-term durability of irradiated concrete. On the other hand, cement paste experiences shrinkage due to (i) the radiolysis process under gamma radiation and (ii) the evaporation of pore water caused by radiation heat [1]. Consequently, the disparity in volumetric changes between concrete components (expansion in aggregates and shrinkage in mortar) can cause damage at the interface between these phases. The different shrinkage properties of aggregates and cement paste can lead to a reduction in concrete compressive strength. The overall volume expansion of the composite compromises its tensile strength, which has been shown to decrease by an average of 62 % and 47 % for flint and limestone aggregates, respectively, within the neutron fluence range of 2×10^{19}–4×10^{19} n/cm^2 [206]. According to Ref. [1], a neutron fluence of less than 10^{19} n/cm^2 does not result in volume increase of irradiated samples; instead, within this range, the volume change is the expected shrinkage due to the temperature exposure of the specimens.

In this context, some studies have reported a reduction in the elastic modulus of concrete, attributing this to the combined effects of neutron-induced damage and heat degradation [207]. However, since concrete is often subjected to constrained conditions, these factors can lead to additional mechanical damage. However, some research reported that gamma radiation generally has not shown significant effects effect on concrete properties, or either improve it in some cases. For example, some research reported excluding radiogenic heating, gamma radiation generally has not shown significant effects on the elastic modulus or the compressive, tensile, or flexural strength of cement products [202,208]. As well, the compressive strength decreased by roughly half at gamma dosages greater than 1 GGy [209]. Soo and Milian [210], reported when radiogenic heating effects are controlled, gamma radiation has no effect on the elastic modulus or the compressive, tensile, or flexural strengths of cement products.

6.2. Durability indicators

The transformation of crystalline quartz into deformed quartz under radiation has two significant negative impacts: microcracking due to volume changes and increased reactivity to aggressive chemicals, such as calcium hydroxide, responsible for alkali–silica reactions (ASR) in concrete. These effects undermine the long-term performance of irradiated concrete [204]. Based on that, it could be said that the durability of RSC subjected to irradiation can be influenced by two key factors: heating (elevated temperature) and the chemical decomposition or reactions triggered by irradiation. Both factors play crucial role in RSC porosity and crack precogitation, consequently effecting the durability. The impact is not necessarily negative in most cases. For example, some studies have notably shown a decrease in concrete porosity when exposed to radiation [211], potentially enhancing its resistance to weathering phenomena involving mass transfer [212]. In addition, it has been noted that concrete porosity decreases under irradiation [211,213], a change that may improve durability against mass transfer weathering events such as carbonation, leaching, sulfate assault, chloride intrusion, alkali–silica reaction, and acid corrosion [212]. This decrease in porosity is hypothesized to be caused by gamma radiation, which promotes the development of aragonite and vaterite instead of calcite during the carbonation process [214].

Relevant studies indicate that gamma radiation refines the pore structure of concrete and reduces the total porosity by around half [211]. This reduction is expected to improve the resistance of concrete to various mass transfer processes by decreasing its permeability and diffusivity [215]. Semiquantitative observation revealed a decrease in the $Ca(OH)_2$ concentration and a rise in the $CaCO_3$ content, which was attributed to gamma radiation accelerating carbonation [208,214]. However, gamma radiation may not significantly accelerate carbonation in high relative humidity situations (about 100 %) and may actually slow carbonation in low humidity situations (around 50 %). Radiation appears to preferentially generate vaterite and aragonite $CaCO_3$ variants over nonirradiated materials. Because vaterite and aragonite are less dense than calcite, this change in carbonate mineral composition may have contributed to the observed decrease in concrete porosity [216].

In terms of influence of heating on RSC, the relevant studies, for instance, indicated that barite concrete experiences a reduction in μ by 12.5 % at 450 °C and 6.4 % at 800 °C, attributed to the expansion of the barite aggregate, leading to cracking and spalling [49,84]. In comparison, magnetite RSC shows a smaller decrease in μ, with reductions of 0.8 % at 600 °C and 3.7 % at 800 °C, likely due to its lower coefficient of thermal expansion [49,92]. Hematite RSC experiences a 6.6 % reduction in μ at 500 °C, whereas serpentine and dolomite RSCs exhibit greater losses of 9.4 % and 13.1 %, respectively, under the same conditions. These reductions are linked to the loss of bonded water, de-hydroxylation and transformation, and the combustion of organic compounds in RSC components, which degrade the material's density and radiation shielding capacity [84,206,217]. The reduction in neutron attenuation is also notable, with coarse barite RSC showing up to a 30 % loss in neutron attenuation ($\sum R(E_n)$) after exposure to 600 °C, primarily due to hydrogen depletion as water evaporates from the material [82]. This issue is compounded in goethite RSC, which records a 35.3 % reduction in $\sum R(E_n)$ after exposure to 450 °C, the most significant loss observed, due to the material's substantial weight loss and hydrogen content reduction [84].

Moreover, the difference in temperature between the surface near the radiation source and the cooler outer surface, as seen in dry cask storage (Fig. 13), can exacerbate cracking through a mechanism similar to that of to that of freeze-thaw cycling. Furthermore, creep may influence the progression of this harm by delaying the appearance of any observable degradation. Briefly, the combination of neutron radiation and high temperatures might induce severe deterioration in concrete utilized as a shielding material, potentially leading to a significant increase in the neutron flux within the concrete. This increase in the neutron flux tends to worsen over time, especially in concrete near the radiation source. Therefore, evaluating the freeze–thaw resistance of RSC is also crucial, particularly in terms of its residual μ after exposure to freeze–thaw cycles. Studies have shown that barite RSC experiences a 25–39 % reduction in μ after 50 freeze–thaw cycles when exposed to a Co-60 source with an average energy of 1.25 MeV. This performance is comparable to natural aggregate concrete, which exhibits a 25–43 % reduction in μ under similar conditions, with the highest residual μ recorded at 0.1 cm−1 for barite concrete and 0.07 cm−1 for natural aggregate concrete [218].

The study [218] further suggests that a higher water-to-cement ratio can mitigate the adverse effects of freeze–thaw cycles on the μ value, as samples with a higher ratio show a lower reduction in μ. The rationale is that a higher water-to-cement ratio increases the free water content in the capillaries and porosity of concrete, which, when frozen, expands and creates internal hydraulic pressure. This pressure, if not dissipated, can exceed the tensile strength of the concrete paste, leading to crack formation. However, the increased porosity in high water-to-cement ratio concrete allows for better dissipation of this pressure, thereby reducing crack formation and maintaining the concrete's shielding properties [219]. Freeze–thaw cycles can damage the microstructure of concrete, potentially compromising its radiation shielding capability. The linear attenuation coefficient, which measures the likelihood of radiation interaction per unit path length, is influenced by factors such as atomic number, incident photon energy, and material density [220]. Numerous studies have explored the linear attenuation coefficients of different concretes. For example, one study calculated these coefficients for concretes with densities over a photon energy range from 10 keV to 1 GeV [137,221], while another examined four grades of concrete within the same photon energy range [222]. Despite the extensive research on concrete, including the effects of freeze–thaw cycles on the mechanical properties of rocks [218,223,224], there remains a significant gap in understanding the impact of freeze–thaw cycles on the radiation shielding characteristics of concrete, highlighting the need for further investigation.

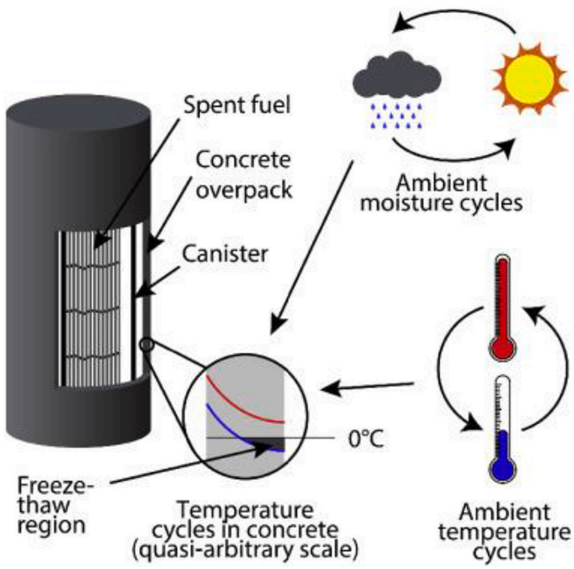

Fig. 13. Environmental conditions and cycles affecting concrete dry casks (Adapted from Ref. [216]).

Research on the chemical attack resistance of RSC is limited. One study on barite RSC revealed a reduction in shielding properties after immersion in sodium sulfate and sodium hydroxide. Specifically, barite RSC retained only about 17 % of its original μ value after six months in sodium hydroxide, with a μ value of 0.35 cm_{-1} at 662 keV from a Cs-137 source. Sodium sulfate had an even more significant adverse effect, reducing the μ value by 28.6 % to about 0.25 cm^{-1} [127]. The study suggests that chemical exposure can severely degrade RSC, especially when the concrete is produced with a high water-to-cement ratio, such as 0.5, leading to increased porosity and vulnerability to chemical attacks [127]. The expansion and increased permeability in RSC due to sulfate attacks, caused by gypsum formation at the interfacial transition zone, further contribute to crack formation and the consequent reduction in shielding properties [225,226].

Another study found that immersion in sodium sulfate for 90 days resulted in a 20.5 % reduction in compressive strength and a 59.5 % reduction in flexural strength of the RSC mortar [227]. Additionally, replacing 50 % of the sand with eggshells led to even greater reductions, with compressive and flexural strengths decreasing by 51.8 % and 10.5 %, respectively. The higher susceptibility of eggshells to sulfate attack, as indicated by a mass loss of 25.7 % compared to 6.3 % for sand mortar, explains these larger reductions. However, the eggshell replacement mixture reported a higher μ value of 3.66 cm^{-1} compared to 1.49 cm^{-1} for sand RSC, based on low-energy Am-241 exposure at 26 keV [227]. This suggests that while RSC with higher porosity or reactive materials is more susceptible to chemical attacks, it may still offer enhanced radiation shielding under certain conditions.

Experimental studies on concrete under gamma irradiation suggest that interactions with radiation reduce both the porosity and strength of the material. The mechanism involves a series of chemical reactions, starting with the radiolysis of water and leading to the formation of $CaCO_3$. Calcite crystallization in the porous structure causes the destruction of tobermorite gel, a key component responsible for concrete strength, through crystallization pressure [227]. Recent research supports this radiolytic process, showing that gamma radiation leads to the amorphization and disintegration of cement hydrates. Scanning electron microscopy and X-ray diffraction techniques have revealed bubbles, likely from chemically bound water separation, and various fractures in the cementitious matrix post-irradiation [228].

6.3. Micro properties

Gamma photon and gamma ray exposure significantly impact the properties and microstructure of cement paste and hydrates. The absorption of gamma photons causes a rise in temperature within the concrete, particularly in environments such as dry casks where the maximum expected temperature can reach approximately 200 °C under worst-case conditions. This temperature distribution varies over time and space, with surfaces closest to spent fuel experiencing the highest temperatures initially, which then decline as the fuel rods decay [216]. Prior studies have noted microstructural changes such as alterations in carbonate speciation linked to reductions in bulk porosity at these radiation levels.

The majority of research on concrete degradation in nuclear settings has concentrated on neutron effects, which are the primary cause of damage in nuclear reactors [229]. However, this does not reflect the situation in dry cask storage [216]. In this scenario, the nuclear source is encased in neutron poison, which substantially mitigates the detrimental effects of neutrons and enhances the prominence of gamma radiation [230]. Radiogenic heating has been investigated as the principal effect of gamma radiation on cementitious products [216], where it was found that this process has detrimental effects on the mechanical properties, mass, and dimensional stability of the products, much like conventional heating [231]. Numerous hypotheses have been proposed regarding the manner in which photons interact with the solid structure of concrete. These include the displacement of atoms within the cementitious phases [84], the disruption of covalent bonds [232], the radiolysis of water [208], the dehydration of cement hydrates [233], and the expansion of aggregates [234].

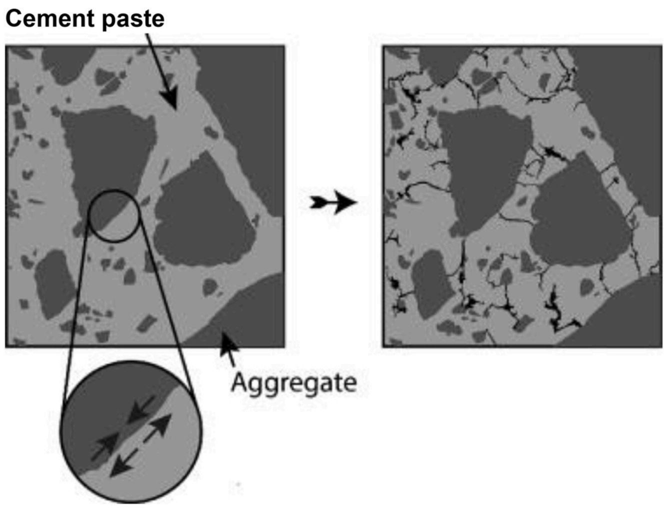

Fig. 14. Developed stress and cracking of concrete induced by heating. a) stresses acting on the ITZ due to differential dehydration shrinkage of the cement paste and thermal expansion of the aggregate, and b) thermal cracking (detailed by Ref. [236] and improved by Ref. [216]).

The elevated temperatures lead to thermal effects on concrete, similar to those observed in fire spalling studies [216,235]. As the temperature increases, water within the concrete's pores and cement hydrates is lost. Specific dehydration processes include the loss of ettringite at 120 °C, progressive dehydration of calcium silicate hydrate (C-S-H) from 120 °C to 800 °C, and dehydration of $Ca(OH)_2$ between 400 and 530 °C [216,235]. These thermal processes induce microstructural stresses and cracks due to the contrasting behaviors of dehydration shrinkage in the cement paste and thermal expansion of aggregates, ultimately reducing the concrete's strength and modulus of elasticity (Fig. 14). These changes occur rapidly, within minutes to hours, and are largely irreversible [216]. Gamma photons also induce several interactions within cement hydrates at the atomic level: dislocation of atoms, breaking and subsequent cross-linking of chemical bonds, hydrolysis of water leading to reactive species formation, and dehydration of chemically bound water due to thermal energy as shown in Fig. 15. These interactions collectively modify the microstructure of cement hydrates, contributing to the degradation of mechanical properties and overall durability of the concrete.

Reportedly, gamma irradiation can cause structural flaws in nano-SiO_2, resulting in a expansion in its particle size [237]. This modification results in a highly reactive and efficient concrete additive. Notably, adding just 1 % (by mass) of nano-SiO_2 irradiated to a level of 100 kGy resulted in more than doubling of the concrete compressive strength. This improvement is consistent with comparable findings in other studies [215]. Gamma rays, a type of ionizing radiation, are hypothesized to disrupt covalent bonds inside cement hydrates, resulting in the formation of radicals [232]. This process may aid in the cross-linking of C-S-H (calcium silicate hydrate) polymers, potentially leading to embrittlement of the overall structure of the concrete [238]. The use of silica nanoparticles as additives to increase the mechanical and durability properties of concrete, particularly at low and high temperatures, has been extensively researched [239]. It is hypothesized that gamma radiation in the 10–150 kGy range can cause flaws in the solid structure of nano-SiO_2, similar to what has been observed in Si-containing aggregates [237]. Overall, it is thought that irradiating nano-SiO_2 may boost its reactivity, enhancing its favorable impact on concrete characteristics [221].

6.4. Alkali–silica reactions

Although not directly related to the alkali-silica reaction (ASR), irradiation can induce a series of chemical reactions that reduce the concrete pore space, decreasing the ability of concrete to absorb pre-expansion ASR gel [211]. It has been reported that the ASR in concrete is initiated by a precise sequence of reactions [240]. First, hydroxide ions in the alkaline solution inside the tiny pores of the concrete react with the silicon dioxide present in the aggregates [237]. This reaction induces the rupture of Si–O bonds, resulting in the expansion of the aggregates as a consequence of this sequence of reactions [1]. As a result of this hydrolysis, OH^- ions are consumed,

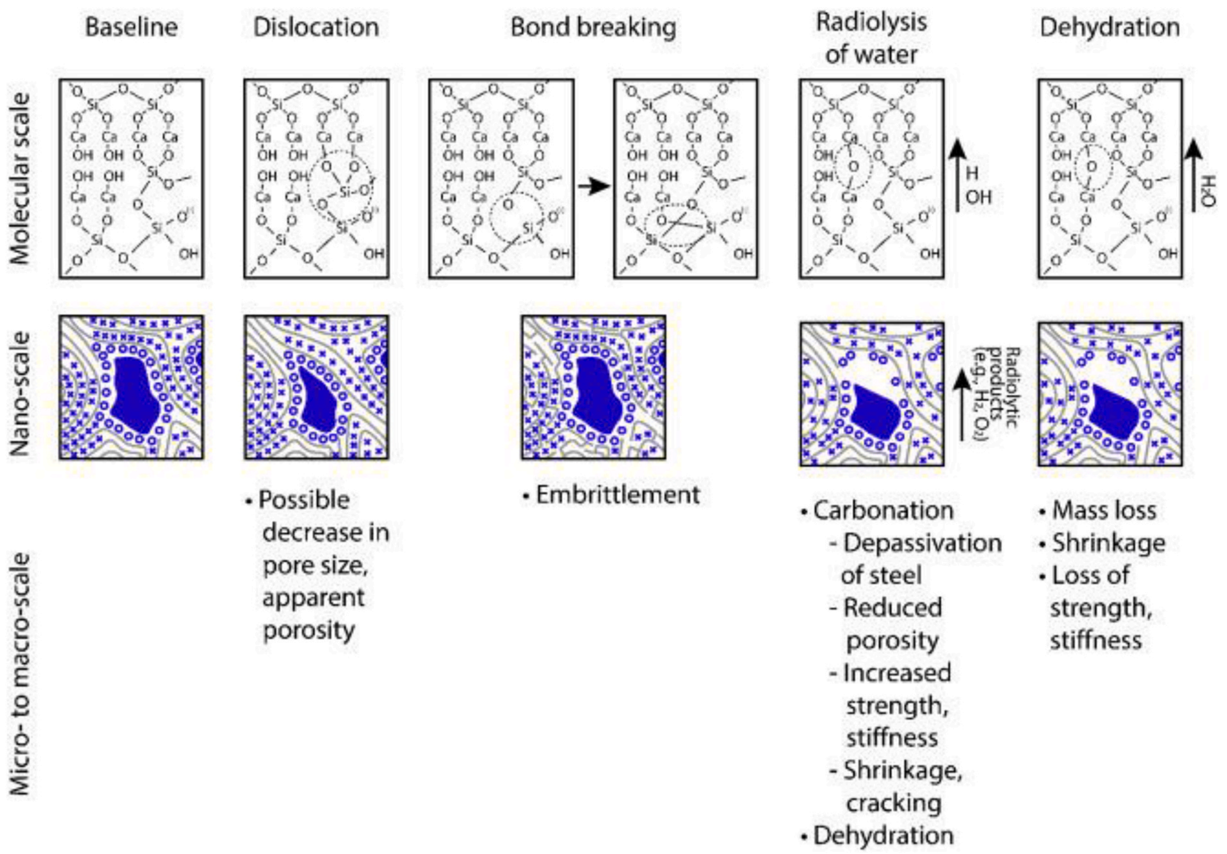

Fig. 15. Mechanisms of interaction between gamma photons and cement hydrates and their multi-scale effects (Adapted from Ref. [216]).

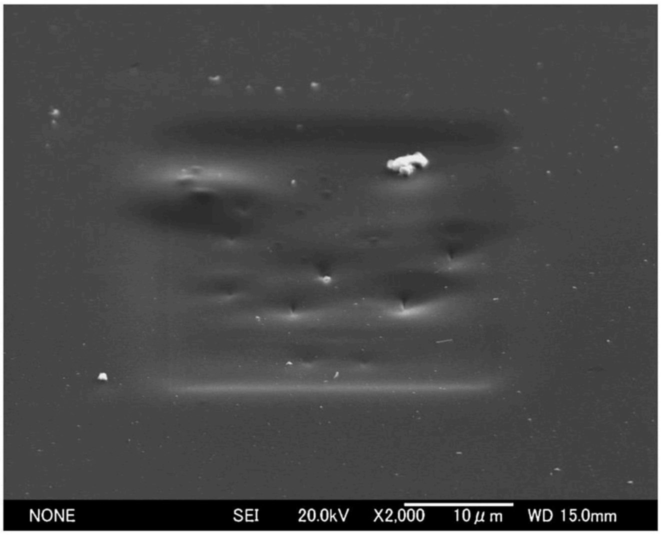

Fig. 16. SEM image of the plagioclase surface after repeated measurements with SEM and electron backscatter diffraction patterns (Adopted from Ref. [240]).

prompting the dissolution of Ca^{2+} ions into the solution [241]. These calcium ions then react with hydrated SiO_2 gels (known as ASR gels) to form calcium silicate [211]. Typically, rigid shells of calcium silicate form on the surface of aggregates as a byproduct of this reaction. Despite the presence of these shells, the alkaline solution can still penetrate the aggregates and dissolve SiO_2 groups [242]. The rigidity of the calcium silicate shells prevents the aggregates from deforming, leading to the buildup of expansion pressure as the solution penetrates [234]. This pressure is confined by the silicate shells, eventually causing cracks and resulting in the final expansion of the aggregates. Fig. 16 displays an SEM image of a crystal surface prior to being exposed to 30 keV electron beam irradiation. The image exhibits a well-defined square located at the center, which corresponds to the region that was consistently examined utilizing a 20 keV electron beam [240]. The cavities in this square were created as a result of extended exposure to concentrated electron beams during electron backscatter diffraction pattern analysis [240,243]. The absence of a diffraction pattern even from the fresh surface suggested that the crystal surface was easily amorphized by the electron beam.

This amorphization results in an increase in density, which explains why repeated SEM imaging caused subsidence of the observed region. Interestingly, this rapid amorphization was not noted in crystalline quartz, indicating that plagioclase is more susceptible to nuclear radiation [240]. Lattice faults in SiO_2 minerals generated by neutron irradiation and aggregate cracks accelerate the ASR in concrete [237]. Research shows that nuclear radiation greatly increases the alkali reactivity of silica-rich aggregates [86]. The SiO_2 content in aggregates correlates with decreased nuclear radiation resistance, strongly accelerating the ASR and causing concrete deterioration. Studies reveal that nuclear irradiation changes the expansion potential of ASR-affected aggregates [213]. The stiffness of the ASR gel affects the free expansion capability of the aggregate and the degree of ASR-related damage. The rigidity of the ASR gel is crucial to this procedure. Soft, low-stiff ASR gel can spread into porous cement paste. Cracking is less likely in such cases due to low swelling pressure [244]. Thus, even a large ASR gel may not damage or cause cracking of the concrete structure [245]. However, even small amounts of stiff ASR gel can cause damage [246]. The ASR gel stiffness depends on its chemical composition, particularly the Na_2O/SiO_2 ratio.

The literature on ASR revealed that radiation has a minimal influence on concrete degradation in the first 40 years of operation in a nuclear power plant [244]. However, extending the structural life of such plants beyond 60–100 years may be useful; however, the existing data are insufficient to completely support these concerns [1]. This issue is especially significant for Seabrook, the first U.S. nuclear plant whose operating license was renewed from 2030 to 2050, which could suffer from ASR. The site has become a focal point for developing an aging management program for older nuclear plants. This initiative highlights the risk of overrelying on surface crack observation and structural component testing while advocating for the development of reliable finite element method-based simulations for long-term structural assessments. In addition to ASR, the aging-related deterioration of concrete materials and components is a high-priority damage source that could affect nuclear plant concrete containment in the long term [247]. Thus, all of these possible challenges must be identified for the future management and safety of aging nuclear power facilities, emphasizing the necessity for continued research and enhanced evaluation procedures.

7. Conclusions and future challenges of RSC

The increasing reliance on nuclear energy and medical radiation technologies has heightened the need for advanced radiation protection solutions. This review provides a comprehensive overview of the developments in concrete materials specifically designed for radiation shielding, highlighting the remaining challenges in the field. The key findings of this review confirm the significant progress has been made in enhancing the shielding capabilities of concrete through the use of dense aggregates, nanoscale fillers, and innovative additives. These materials have demonstrated effectiveness in blocking various types of radiation, making RSC a superior alternative to traditional shielding materials like lead. RSC offers exceptional shielding properties, cost-effectiveness, and the ability to be tailored for specific applications. However, several critical areas require further research and development to ensure that RSC meets future demands and remains a viable long-term solution. Key areas requiring further research can be summarized as following:

❖ The stability of hematite-containing concrete at elevated temperatures requires further exploration.
❖ While the relationship between concrete density, heavyweight aggregates, and radiation shielding is well-studied, there is a lack of research on how the percentage of added materials affects γ-ray attenuation in concrete.
❖ More research is needed on how photons interact with concrete's microstructural phases, including atom displacement, covalent bond disruption, water radiolysis, cement hydrate dehydration, and aggregate expansion.
❖ Chemically pre-treated fibers offer potential for improving concrete's neutron shielding properties, representing a promising research area.
❖ Investigating the durability and performance of RSCs under extreme conditions, such as high temperatures, moisture, and radiation exposure, is crucial.
❖ Research on the combined shielding protection provided by nanoparticles against gamma and neutron radiation in RSC is limited and requires further exploration.
❖ Research on the use of supplementary cementitious materials in RSC production is scarce, indicating a significant gap in the literature.
❖ There is a need for more studies assessing the impact of irradiation on the mechanical performance and properties of concrete after exposure, as current research predominantly focuses on comparing the effectiveness of additives in enhancing radiation shielding.
❖ A comprehensive analysis of the complete lifecycle of RSCs—from raw material extraction to disposal—focusing on environmental and cost impacts, is necessary to ensure sustainability.

CRediT authorship contribution statement

Ali M. Onaizi: Writing – review & editing, Writing – original draft, Visualization, Validation, Software, Resources, Formal analysis, Data curation, Conceptualization. **Mugahed Amran:** Writing – review & editing, Writing – original draft, Visualization, Validation, Supervision, Software, Investigation, Conceptualization. **Waiching Tang:** Writing – review & editing, Visualization, Supervision, Investigation, Data curation, Conceptualization. **Nour Betoush:** Writing – review & editing, Software. **Mohammad Alhassan:** Writing – review & editing, Supervision, Conceptualization. **Raizal S.M. Rashid:** Writing – review & editing, Supervision.**Mohammad Fares Yasin:** Writing – review & editing. **K.H. Bayagoob:** Writing – review & editing, Supervision. **Sagheer A. Onaizi:** Writing – review & editing, Supervision, Conceptualization.

Declaration of competing interest

The authors declare that they have no known competing financial interests or personal relationships that could have appeared to influence the work reported in this paper.

Data availability

Data will be made available on request.

Acknowledgments

The authors gratefully acknowledge the assistance and cooperation provided by the University of Newcastle for this work.

References

[1] B. Pomaro, A review on radiation damage in concrete for nuclear facilities: from experiments to modeling, Model. Simulat. Eng. 2016 (2016), https://doi.org/10.1155/2016/4165746.
[2] Roddis LH. Nuclear power in the world today n.d.;2. https://doi.org/10.1109/MSPEC.1965.5531714.
[3] World Nuclear Association, 2014. World nuclear power reactors and uranium requirements. World Nuclear Association, London. Available at: https://world-nuclear.org/information-library/facts-and-figures/world-nuclear-power-reactors-archive/reactor-archive-january-2014 [Accessed 21 July 2024].
[4] K. Park, H.T. Kim, T.H. Kwon, E. Choi, Effect of neutron irradiation on response of reinforced concrete members for nuclear power plants, Nucl. Eng. Des. 310 (2016) 15–26, https://doi.org/10.1016/j.nucengdes.2016.09.034.
[5] K. Sadamori, Nuclear power in a clean energy system, Ann Des Mines - Responsab Environ. (2019) 122–126, https://doi.org/10.3917/re1.097.0122.
[6] IEA-agency, Cumulative CO2 emissions avoided by nuclear power by country, 1990-2020, Int Energy Agency Website 1 (2019).
[7] R. Michal, Fifty years ago in December : atomic reactor EBR-I produced first electricity, Nucl. News 44 (2001) 28–29.
[8] P. Gummett, Global fission: the battle over nuclear power, Phys. Bull. 35 (1984) 518, https://doi.org/10.1088/0031-9112/35/12/024.
[9] S.J. Jepeal, L. Snead, Z.S. Hartwig, Intermediate energy proton irradiation: rapid, high-fidelity materials testing for fusion and fission energy systems, Mater. Des. 200 (2021), https://doi.org/10.1016/j.matdes.2020.109445.
[10] Y. Maki, H. Ohnuma, Application of concrete to the treatment and disposal of radioactive waste in Japan, Nucl. Eng. Des. 138 (1992) 179–188, https://doi.org/10.1016/0029-5493(92)90294-6.
[11] C.C. Ban, M.A. Khalaf, M. Ramli, N.M. Ahmed, M.S. Ahmad, A.M.A. Ali, et al., Modern heavyweight concrete shielding: principles, industrial applications and future challenges; review, J. Build. Eng. 39 (2021) 102290.
[12] B. Kanagaraj, N. Anand, A. Diana Andrushia, M.Z. Naser, Recent developments of radiation shielding concrete in nuclear and radioactive waste storage facilities – a state of the art review, Construct. Build. Mater. 404 (2023) 133260, https://doi.org/10.1016/j.conbuildmat.2023.133260.
[13] M.S. Al-Buriahi, J.S. Alzahrani, Z.A. Alrowaili, I.O. Olarinoye, C. Sriwunkum, Recycling of waste cathode-ray tube glasses as building materials for shielding structures in medical and nuclear facilities, Construct. Build. Mater. 376 (2023) 131029.

[14] P. Zhang, F.H. Wittmann, T. Zhao, E.H. Lehmann, P. Vontobel, Neutron radiography, a powerful method to determine time-dependent moisture distributions in concrete, Nucl. Eng. Des. 241 (2011) 4758–4766.
[15] A.M. Zayed, A.M. El-Khayatt, P. Petrounias, M.G. Shahien, K.A. Mahmoud, A.M. Rashad, et al., From discarded waste to valuable products: barite combination with chrysotile mine waste to produce radiation-shielding concrete, Construct. Build. Mater. 417 (2024) 135334.
[16] D.S. Wisnubroto, H. Zamroni, R. Sumarbagiono, G. Nurliati, Challenges of implementing the policy and strategy for management of radioactive waste and nuclear spent fuel in Indonesia, Nucl. Eng. Technol. 53 (2021) 549–561.
[17] World Nuclear Association, Nuclear power in the world today. https://world-nuclear.org/information-library/current-and-future-generation/nuclear-power-in-the-world-today#:~:text=Nuclear-energy-now-provides-about-source-of-low-carbon-power, 2024.
[18] H.E. Hassan, H.M. Badran, A. Aydarous, T. Sharshar, Studying the effect of nano lead compounds additives on the concrete shielding properties for γ-rays, Nucl. Instrum. Methods Phys. Res. Sect. B Beam Interact. Mater. Atoms 360 (2015) 81–89, https://doi.org/10.1016/j.nimb.2015.07.126.
[19] IAEA. Iaea Safety Glossary, Int at Energy Agency, 2016, p. 219. Vienna.
[20] E. Al-sarray, INVESTIGATION OF RADIATION SHIELDING PROPERTIES OF SOME COMPOSITE MATERIALS, 2016.
[21] M.U. Khan, S. Ahmad, A.A. Naqvi, H.J. Al-Gahtani, Shielding performance of heavy-weight ultra-high-performance concrete against nuclear radiation, Prog. Nucl. Energy 130 (2020) 103550, https://doi.org/10.1016/j.pnucene.2020.103550.
[22] T. Daungwilailuk, C. Yenchai, W. Rungjaroenkiti, P. Pheinsusom, C. Panwisawas, W. Pansuk, Use of barite concrete for radiation shielding against gamma-rays and neutrons, Construct. Build. Mater. 326 (2022), https://doi.org/10.1016/j.conbuildmat.2022.126838.
[23] K. Apte, S. Bhide, Basics of Radiation, Adv. Radiat. Shield. Mater., Elsevier, 2024, pp. 1–23.
[24] T. Piotrowski, Neutron shielding evaluation of concretes and mortars: a review, Construct. Build. Mater. 277 (2021), https://doi.org/10.1016/j.conbuildmat.2020.122238.
[25] P. Prochon, T. Piotrowski, The effect of cement and aggregate type and w/c ratio on the bound water content and neutron shielding efficiency of concretes, Construct. Build. Mater. 264 (2020) 120210.
[26] M.A. Glinicki, A. Antolik, M. Gawlicki, Evaluation of compatibility of neutron-shielding boron aggregates with Portland cement in mortar, Construct. Build. Mater. 164 (2018) 731–738, https://doi.org/10.1016/j.conbuildmat.2017.12.228.
[27] A. Cato, L. Sutton, I.I.I.A. Cato, Radiation detection and measurement, Radiat. Saf. Nucl. Med. (2021) 81–104, https://doi.org/10.1201/9780849381799-7.
[28] M.A. Masoud, W.A. Kansouh, M.G. Shahien, K. Sakr, A.M. Rashad, A.M. Zayed, An experimental investigation on the effects of barite/hematite on the radiation shielding properties of serpentine concretes, Prog. Nucl. Energy 120 (2020) 103220, https://doi.org/10.1016/j.pnucene.2019.103220.
[29] I.I. Bashter, A. El-Sayed Abdo, A.S. Makarious, A comparative study of the attenuation of reactor thermal neutrons in different types of concrete, Ann. Nucl. Energy 23 (1996) 1189–1195, https://doi.org/10.1016/0306-4549(95)00122-0.
[30] M. Alwaeli, J. Nadziakiewicz, Recycling of scale and steel chips waste as a partial replacement of sand in concrete, Construct. Build. Mater. 28 (2012) 157–163, https://doi.org/10.1016/j.conbuildmat.2011.08.047.
[31] O. Gencel, A. Bozkurt, E. Kam, T. Korkut, Determination and calculation of gamma and neutron shielding characteristics of concretes containing different hematite proportions, Ann. Nucl. Energy 38 (2011) 2719–2723, https://doi.org/10.1016/j.anucene.2011.08.010.
[32] B. Oto, A. Gür, M.R. Kaçal, B. Doğan, A. Arasoglu, Photon attenuation properties of some concretes containing barite and colemanite in different rates, Ann. Nucl. Energy 51 (2013) 120–124, https://doi.org/10.1016/j.anucene.2012.06.033.
[33] B. Oto, A. Gür, Determination of mass attenuation coefficients of concretes containing ulexite and ulexite concentrator waste, Ann. Nucl. Energy 59 (2013) 72–74, https://doi.org/10.1016/j.anucene.2013.03.018.
[34] N. Yaltay, C.E. Ekinci, T. Çakir, B. Oto, Photon attenuation properties of concrete produced with pumice aggregate and colemanite addition in different rates and the effect of curing age to these properties, Prog. Nucl. Energy 78 (2015) 25–35, https://doi.org/10.1016/j.pnucene.2014.08.002.
[35] K. Sakr, E. El-Hakim, Effect of high temperature or fire on heavy weight concrete properties, Cement Concr. Res. 35 (2005) 590–596, https://doi.org/10.1016/j.cemconres.2004.05.023.
[36] N. Singh, K.J. Singh, K. Singh, H. Singh, Gamma-ray attenuation studies of PbO-BaO-B2O3 glass system, Radiat. Meas. 41 (2006) 84–88, https://doi.org/10.1016/j.radmeas.2004.09.009.
[37] M.A. Masoud, A.M. El-Khayatt, W.A. Kansouh, K. Sakr, M.G. Shahien, A.M. Zayed, Insights into the effect of the mineralogical composition of serpentine aggregates on the radiation attenuation properties of their concretes, Construct. Build. Mater. 263 (2020), https://doi.org/10.1016/j.conbuildmat.2020.120141.
[38] A.E. Abdo, M.A. El-sarraf, F.A. Gaber, Utilization of Ilmenite/Epoxy Composite for Neutrons and Gamma Rays Attenuation, vol. 30, 2003, pp. 175–187.
[39] I. Akkurt, H. Akyildirim, B. Mavi, S. Kilincarslan, C. Basyigit, Radiation shielding of concrete containing zeolite, Radiat. Meas. 45 (2010) 827–830, https://doi.org/10.1016/j.radmeas.2010.04.012.
[40] S.M. Rasoul Abdar Esfahani, S.A. Zareei, M. Madhkhan, F. Ameri, J. Rashidiani, R.A. Taheri, Mechanical and gamma-ray shielding properties and environmental benefits of concrete incorporating GGBFS and copper slag, J. Build. Eng. 33 (2021), https://doi.org/10.1016/j.jobe.2020.101615.
[41] F. Demir, G. Budak, R. Sahin, A. Karabulut, M. Oltulu, A. Un, Determination of radiation attenuation coefficients of heavyweight- and normal-weight concretes containing colemanite and barite for 0.663 MeV γ-rays, Ann. Nucl. Energy 38 (2011) 1274–1278, https://doi.org/10.1016/j.anucene.2011.02.009.
[42] E. Yilmaz, H. Baltas, E. Kiris, I. Ustabas, U. Cevik, A.M. El-Khayatt, Gamma ray and neutron shielding properties of some concrete materials, Ann. Nucl. Energy 38 (2011) 2204–2212, https://doi.org/10.1016/j.anucene.2011.06.011.
[43] W.M. Al-Saleh, H.M. Almutairi, M.I. Sayyed, M. Elsafi, Multilayer radiation shielding system with advanced composites containing heavy metal oxide nanoparticles: a free-lead solution, Sci. Rep. 13 (2023) 18429.
[44] S. Xu, M. Bourham, A. Rabiei, A novel ultra-light structure for radiation shielding, Mater. Des. 31 (2010) 2140–2146, https://doi.org/10.1016/j.matdes.2009.11.011.
[45] M.I. Sayyed, N. Almousa, M. Elsafi, Preparation of mortar with Fe2O3 nanoparticles for radiation shielding application, Coatings 12 (2022), https://doi.org/10.3390/coatings12091329.
[46] M.H. Kharita, S. Yousef, M. AlNassar, The effect of carbon powder addition on the properties of hematite radiation shielding concrete, Prog. Nucl. Energy 51 (2009) 388–392, https://doi.org/10.1016/j.pnucene.2008.10.002.
[47] M.H. Kharita, S. Yousef, M. AlNassar, The effect of the initial water to cement ratio on shielding properties of ordinary concrete, Prog. Nucl. Energy 52 (2010) 491–493, https://doi.org/10.1016/j.pnucene.2009.11.005.
[48] M.H. Kharita, S. Yousef, M. Alnassar, Review on the addition of boron compounds to radiation shielding concrete, Prog. Nucl. Energy 53 (2011) 207–211, https://doi.org/10.1016/j.pnucene.2010.09.012.
[49] E. Horszczaruk, P. Brzozowski, Investigation of gamma ray shielding efficiency and physicomechanical performances of heavyweight concrete subjected to high temperature, Construct. Build. Mater. 195 (2019) 574–582, https://doi.org/10.1016/j.conbuildmat.2018.09.113.
[50] M.A. El-Nahal, M. Elsafi, M.I. Sayyed, M.U. Khandaker, H. Osman, B.H. Elesawy, et al., Understanding the effect of introducing micro- and nanoparticle bismuth oxide (Bi2O3) on the gamma ray shielding performance of novel concrete, Materials 14 (2021), https://doi.org/10.3390/ma14216487.
[51] B. Pomaro, F. Gramegna, R. Cherubini, V. De Nadal, V. Salomoni, F. Faleschini, Gamma-ray shielding properties of heavyweight concrete with Electric Arc Furnace slag as aggregate: an experimental and numerical study, Construct. Build. Mater. 200 (2019) 188–197, https://doi.org/10.1016/j.conbuildmat.2018.12.098.
[52] D. Rezaei Ochbelagh, S. Azimkhani, H. Gasemzadeh Mosavinejad, Effect of gamma and lead as an additive material on the resistance and strength of concrete, Nucl. Eng. Des. 241 (2011) 2359–2363, https://doi.org/10.1016/j.nucengdes.2011.03.001.
[53] A.S. Ouda, Development of high-performance heavy density concrete using different aggregates for gamma-ray shielding, HBRC J 11 (2015) 328–338, https://doi.org/10.1016/j.hbrcj.2014.06.010.
[54] I.M. Nikbin, M. Shad, G.A. Jafarzadeh, S. Dezhampanah, An experimental investigation on combined effects of nano-WO3 and nano-Bi2O3 on the radiation shielding properties of magnetite concretes, Prog. Nucl. Energy 117 (2019), https://doi.org/10.1016/j.pnucene.2019.103103.

[55] D. Rezaei-Ochbelagh, S. Azimkhani, Investigation of gamma-ray shielding properties of concrete containing different percentages of lead, Appl. Radiat. Isot. 70 (2012) 2282–2286, https://doi.org/10.1016/j.apradiso.2012.06.020.
[56] A. Radziejowska, J. Sagan, A. Sobotka, Technological and organizational problems in the construction of the radiation shielding concrete and suggestions to solve: a case study, Open Eng. 11 (2021) 1122–1129, https://doi.org/10.1515/eng-2021-0082.
[57] G. Tyagi, A. Singhal, S. Routroy, D. Bhunia, M. Lahoti, Radiation Shielding Concrete with alternate constituents: an approach to address multiple hazards, J. Hazard Mater. 404 (2021), https://doi.org/10.1016/j.jhazmat.2020.124201.
[58] M. Çullu, E. Bakirhan, Investigation of radiation absorption coefficients of lead-zinc mine waste rock mixed heavy concrete at 662–1460 keV energy range, Construct. Build. Mater. 173 (2018) 17–27, https://doi.org/10.1016/j.conbuildmat.2018.03.175.
[59] Universalmedicalinc. 3 Different Types of Radiation Shielding Materials. Globe Compos Solut LLC (n.d.).
[60] A. Anshul, S.S. Amritphale, N. Chandra, N. Ramakrishnan, A. Shrivastava, U.S.P.P. Verma, Chemically formulated ceramic gamma ray irradiation shielding materials utilising red mud, Adv. Appl. Ceram. 108 (2009) 429–437, https://doi.org/10.1179/174367609X414017.
[61] J. Patočka, K. Kuča, Lead exposure and environmental health, Mil Med. Sci. Lett. 85 (2016) 147–163, https://doi.org/10.31482/mmsl.2016.027.
[62] T. Kaur, J. Sharma, T. Singh, Review on scope of metallic alloys in gamma rays shield designing, Prog. Nucl. Energy 113 (2019) 95–113, https://doi.org/10.1016/j.pnucene.2019.01.016.
[63] B. Aygün, E. Şakar, E. Cinan, N.Y. Yorgun, M.I. Sayyed, O. Agar, et al., Development and production of metal oxide doped glasses for gamma ray and fast neutron shielding, Radiat. Phys. Chem. 174 (2020), https://doi.org/10.1016/j.radphyschem.2020.108897.
[64] G. Tyagi, A. Singhal, S. Routroy, D. Bhunia, M. Lahoti, A review on sustainable utilization of industrial wastes in radiation shielding concrete, Mater. Today Proc. (2020), https://doi.org/10.1016/j.matpr.2020.03.474.
[65] M. Afiq, H. Abdullah, R. Saifulnaz, M. Rashid, M. Amran, F. Hejazii, et al., Recent trends in advanced radiation shielding concrete for construction of facilities : materials and properties, Polymers 14 (2022) 2830.
[66] K. Mokhtari, M. Kheradmand Saadi, H. Ahmadpanahi, G. Jahanfarnia, Fabrication, characterization, simulation and experimental studies of the ordinary concrete reinforced with micro and nano lead oxide particles against gamma radiation, Nucl. Eng. Technol. 53 (2021) 3051–3057, https://doi.org/10.1016/j.net.2021.04.001.
[67] A.L. Beaucour, P. Pliya, F. Faleschini, R. Njinwoua, C. Pellegrino, A. Noumowé, Influence of elevated temperature on properties of radiation shielding concrete with electric arc furnace slag as coarse aggregate, Construct. Build. Mater. 256 (2020), https://doi.org/10.1016/j.conbuildmat.2020.119385.
[68] J. Li, C. Wu, H. Hao, Z. Wang, Y. Su, Experimental investigation of ultra-high performance concrete slabs under contact explosions, Int. J. Impact Eng. 93 (2016) 62–75, https://doi.org/10.1016/j.ijimpeng.2016.02.007.
[69] I. Shafiq, M. Azreen, M.W. Hussin, Sulphuric Acid Resistant of Self Compacted Geopolymer Concrete Containing Slag and Ceramic Waste, MATEC Web Conf., 2017, https://doi.org/10.1051/matecconf/20179701102.
[70] W.A. Kansouh, Radiation distribution through serpentine concrete using local materials and its application as a reactor biological shield, Ann. Nucl. Energy 47 (2012) 258–263, https://doi.org/10.1016/j.anucene.2012.05.008.
[71] P. Sikora, M. Abd Elrahman, E. Horszczaruk, P. Brzozowski, D. Stephan, Incorporation of magnetite powder as a cement additive for improving thermal resistance and gamma-ray shielding properties of cement-based composites, Construct. Build. Mater. 204 (2019) 113–121, https://doi.org/10.1016/j.conbuildmat.2019.01.161.
[72] N.M. Azreen, R.S.M. Rashid, M. Haniza, Y.L. Voo, Y.H. Mugahed Amran, Radiation shielding of ultra-high-performance concrete with silica sand, amang and lead glass, Construct. Build. Mater. 172 (2018) 370–377, https://doi.org/10.1016/j.conbuildmat.2018.03.243.
[73] N.M. Azreen, R.S.M. Rashid, Y.H. Mugahed Amran, Y.L. Voo, M. Haniza, M. Hairie, et al., Simulation of ultra-high-performance concrete mixed with hematite and barite aggregates using Monte Carlo for dry cask storage, Construct. Build. Mater. 263 (2020), https://doi.org/10.1016/j.conbuildmat.2020.120161.
[74] M.A. El-Sarraf, Abdo A. El-Sayed, Influence of magnetite, ilmenite and boron carbide on radiation attenuation of polyester composites, Radiat. Phys. Chem. 88 (2013) 21–26, https://doi.org/10.1016/j.radphyschem.2013.03.003.
[75] A.S. Mollah, Evaluation of gamma radiation attenuation characteristics of different type shielding materials used in nuclear medicine services. Bangladesh, J. Nucl. Med. 21 (2019) 108–114, https://doi.org/10.3329/bjnm.v21i2.40361.
[76] M.M. Al-humaiqani, A.B. Shuraim, R.R. Hussain, γ -radiation shielding properties of high strength high performance concretes prepared with different types of normal and heavy aggregates, Asian Trans. Eng. 3 (2013) 18–28.
[77] The Concrete Society, Heavyweight concrete, Concr. Soc. Webside 1 (2018).
[78] E. Zorla, C. Ipbüker, A. Biland, M. Kiisk, S. Kovaljov, A.H. Tkaczyk, et al., Radiation shielding properties of high performance concrete reinforced with basalt fibers infused with natural and enriched boron, Nucl. Eng. Des. 313 (2017) 306–318, https://doi.org/10.1016/j.nucengdes.2016.12.029.
[79] A.S. Ouda, Estimation of radiation properties of high-performance concrete for use in nuclear installations, J. Mater. Civ. Eng. 28 (2016) 04016121, https://doi.org/10.1061/(asce)mt.1943-5533.0001638.
[80] A. Mesbahi, H. Ghiasi, Shielding properties of the ordinary concrete loaded with micro- and nano-particles against neutron and gamma radiations, Appl. Radiat. Isot. 136 (2018) 27–31, https://doi.org/10.1016/j.apradiso.2018.02.004.
[81] G. Lakshminarayana, S.O. Baki, K.M. Kaky, M.I. Sayyed, H.O. Tekin, A. Lira, et al., Investigation of structural, thermal properties and shielding parameters for multicomponent borate glasses for gamma and neutron radiation shielding applications, J. Non-Cryst. Solids 471 (2017) 222–237, https://doi.org/10.1016/j.jnoncrysol.2017.06.001.
[82] Gumus M. Demir, H.S. Gokce, Gamma ray and neutron shielding characteristics of polypropylene fiber-reinforced heavyweight concrete exposed to high temperatures, Construct. Build. Mater. 257 (2020), https://doi.org/10.1016/j.conbuildmat.2020.119596.
[83] M. Tuyan, H.S. Gökçe, Optimization of reactive powder concrete by means of barite aggregate for both neutrons and gamma rays. https://doi.org/10.1016/j.conbuildmat.2018.09.022, 2018.
[84] M.G. El-Samrah, M.A.E. Abdel-Rahman, R.M. El Shazly, Effect of heating on physical, mechanical, and nuclear radiation shielding properties of modified concrete mixes, Radiat. Phys. Chem. 153 (2018) 104–110, https://doi.org/10.1016/j.radphyschem.2018.09.018.
[85] R.S.M. Rashid, S.M. Salem, N.M. Azreen, Y.L. Voo, M. Haniza, A.A. Shukri, et al., Effect of elevated temperature to radiation shielding of ultra-high performance concrete with silica sand or magnetite, Construct. Build. Mater. 262 (2020) 120567, https://doi.org/10.1016/j.conbuildmat.2020.120567.
[86] D. Han, W. Kim, S. Lee, H. Kim, P. Romero, Assessment of gamma radiation shielding properties of concrete containers containing recycled coarse aggregates, Construct. Build. Mater. 163 (2018) 122–138, https://doi.org/10.1016/j.conbuildmat.2017.12.078.
[87] O. Lotfi-Omran, A. Sadrmomtazi, I.M. Nikbin, A comprehensive study on the effect of water to cement ratio on the mechanical and radiation shielding properties of heavyweight concrete, Construct. Build. Mater. 229 (2019), https://doi.org/10.1016/j.conbuildmat.2019.116905.
[88] F. Ameri, J. de Brito, M. Madhkhan, R.A. Taheri, Steel fibre-reinforced high-strength concrete incorporating copper slag: mechanical, gamma-ray shielding, impact resistance, and microstructural characteristics, J. Build. Eng. 29 (2020), https://doi.org/10.1016/j.jobe.2019.101118.
[89] M.E. Mahmoud, M. El-Sharkawy R, E.A. Allam, R. Elsaman, A. El-Taher, Fabrication and characterization of phosphotungstic acid - copper oxide nanoparticles - plastic waste nanocomposites for enhanced radiation-shielding, J. Alloys Compd. 803 (2019) 768–777, https://doi.org/10.1016/j.jallcom.2019.06.290.
[90] D.E. Tobbala, Effect of Nano-ferrite addition on mechanical properties and gamma ray attenuation coefficient of steel fiber reinforced heavy weight concrete, Construct. Build. Mater. 207 (2019) 48–58, https://doi.org/10.1016/j.conbuildmat.2019.02.099.
[91] S.A. Abo-El-Enein, F.I. El-Hosiny, S.M.A. El-Gamal, M.S. Amin, M. Ramadan, Gamma radiation shielding, fire resistance and physicochemical characteristics of Portland cement pastes modified with synthesized Fe2O3 and ZnO nanoparticles, Construct. Build. Mater. 173 (2018) 687–706, https://doi.org/10.1016/j.conbuildmat.2018.04.071.
[92] I.M. Nikbin, S. Mehdipour, S. Dezhampanah, R. Mohammadi, R. Mohebbi, H.H. Moghadam, et al., Effect of high temperature on mechanical and gamma ray shielding properties of concrete containing nano-TiO2, Radiat. Phys. Chem. 174 (2020), https://doi.org/10.1016/j.radphyschem.2020.108967.
[93] R. Florez, H.A. Colorado, A. Alajo, C.H.C. Giraldo, The material characterization and gamma attenuation properties of Portland cement-Fe3O4 composites for potential dry cask applications, Prog. Nucl. Energy 111 (2019) 65–73, https://doi.org/10.1016/j.pnucene.2018.10.022.

[94] M. Alwaeli, Investigation of gamma radiation shielding and compressive strength properties of concrete containing scale and granulated lead-zinc slag wastes, J. Clean. Prod. 166 (2017) 157–162, https://doi.org/10.1016/j.jclepro.2017.07.203.
[95] Y. Yao, X. Zhang, M. Li, R. Yang, T. Jiang, J. Lv, Investigation of gamma ray shielding efficiency and mechanical performances of concrete shields containing bismuth oxide as an environmentally friendly additive, Radiat. Phys. Chem. 127 (2016) 188–193, https://doi.org/10.1016/j.radphyschem.2016.06.028.
[96] M. Papachristoforou, I. Papayianni, Radiation shielding and mechanical properties of steel fiber reinforced concrete (SFRC) produced with EAF slag aggregates, Radiat. Phys. Chem. 149 (2018) 26–32, https://doi.org/10.1016/j.radphyschem.2018.03.010.
[97] J. Baalamurugan, V. Ganesh Kumar, S. Chandrasekaran, S. Balasundar, B. Venkatraman, R. Padmapriya, et al., Utilization of induction furnace steel slag in concrete as coarse aggregate for gamma radiation shielding, J. Hazard Mater. 369 (2019) 561–568, https://doi.org/10.1016/j.jhazmat.2019.02.064.
[98] M. Awadeen, M. Amin, R.H. Bakr, A.M. Tahwia, Mechanical properties, attenuation coefficient, and microstructure of ultra high-performance heavyweight concrete for radiation shielding applications, J. Build. Eng. 82 (2024) 108395, https://doi.org/10.1016/j.jobe.2023.108395.
[99] M. Amin, W.E. Elemam, M.A. Kandil, M. Samy, Effect of heavy-weight recycled materials on radiation shielding and properties of high-strength concrete with CEM III, J. Build. Eng. 79 (2023) 107819, https://doi.org/10.1016/j.jobe.2023.107819.
[100] S. Dezhampanah, I.M. Nikbin, S. Mehdipour, R. Mohebbi, H. Moghadam, Fiber- reinforced concrete containing nano - TiO2 as a new gamma-ray radiation shielding materials, J. Build. Eng. 44 (2021) 102542, https://doi.org/10.1016/j.jobe.2021.102542.
[101] H.S. Gokce, B.C. Ozturk, N.F. Çam, Ö. Andic-Cakir, Gamma-ray attenuation coefficients and transmission thickness of high consistency heavyweight concrete containing mineral admixture, Cem. Concr. Compos. 92 (2018) 56–69, https://doi.org/10.1016/j.cemconcomp.2018.05.015.
[102] E. Miller, High density and radiation shielding concrete and grout, Adv Concr Technol (2003) 1–15.
[103] M.E. Mitwally, A. Elnemr, A. Shash, A. Babiker, Utilization of steel slag as partial replacement for coarse aggregate in concrete, Innov. Infrastruct. Solut. 9 (2024) 175, https://doi.org/10.1007/s41062-024-01464-y.
[104] A. Hassan, A. ElNemr, L. Goebel, C. Koenke, Effect of hybrid polypropylene fibers on mechanical and shrinkage behavior of alkali-activated slag concrete, Construct. Build. Mater. 411 (2024) 134485, https://doi.org/10.1016/j.conbuildmat.2023.134485.
[105] F.A. Bouzarjomehri, T. Bayat, R. Dashti, J. Gheysari, N. Abdoli, 60Co Y-Ray Attenuation Coefficient of Barite Concrete, 2006.
[106] U. Ulusoy, Comparison of particle shapes of conventionally ground barite, calcite and talc minerals by dynamic imaging technique: a review, EUREKA Phys. Eng. 5 (2020) 80–90.
[107] I. Lakatos, J. Lakatos-Szabo, B. Kosztin, Comparative Study of Different Barite Dissolvers: Technical and Economic Aspects, SPE Int. Conf. Exhib. Form. Damage Control, SPE, 2002, pp. SPE–73719.
[108] G.G. Del Angel, A. Aghajanian, P. Tamayo, J. Rico, C. Thomas, Siderurgical aggregate cement-treated bases and concrete using foundry sand, Appl. Sci. 11 (2021) 435.
[109] P. Tamayo, C. Thomas, J. Rico, S. Pérez, A. Mañanes, Radiation shielding properties of siderurgical aggregate concrete, Construct. Build. Mater. 319 (2022), https://doi.org/10.1016/j.conbuildmat.2021.126098.
[110] R. Şahin, R. Polat, O. Içelli, C. Çelik, Determination of transmission factors of concretes with different water/cement ratio, curing condition, and dosage of cement and air entraining agent, Ann. Nucl. Energy 38 (2011) 1505–1511, https://doi.org/10.1016/j.anucene.2011.03.013.
[111] M. Dong, S. Zhou, X. Xue, X. Feng, M.I. Sayyed, M.U. Khandaker, et al., The potential use of boron containing resources for protection against nuclear radiation, Radiat. Phys. Chem. 188 (2021) 109601.
[112] S. Demirci, M.S. Kaya, A. Doğan, Ş. Kalay, N.Ö. Altin, A. Yarat, et al., Antibacterial and cytotoxic properties of boron-containing dental composite, Turkish J. Biol. 39 (2015) 417–426.
[113] I.D. Giovannelli-Maizo, A.P. Luz, V.C. Pandolfelli, Advanced boron-containing refractory castables bonded with calcium-free binders, Ceram. Int. 45 (2019) 8774–8782.
[114] A. Levet, E. Kavaz, Y. Özdemir, An experimental study on the investigation of nuclear radiation shielding characteristics in iron-boron alloys, J. Alloys Compd. 819 (2020) 152946.
[115] M. Mursalat, H. McCann, M. Schoenitz, E.L. Dreizin, Effect of particle morphology on characteristics of pressed aluminum-boron reactive powders, J. Energetic Mater. (2022) 1–13.
[116] A.M. Zeyad, I.Y. Hakeem, M. Amin, B.A. Tayeh, I.S. Agwa, Effect of aggregate and fibre types on ultra-high-performance concrete designed for radiation shielding, J. Build. Eng. 58 (2022) 104960.
[117] P. Kongsat, S. Sinthupinyo, E.A. O'Rear, T. Pongprayoon, Effect of morphologically controlled hematite nanoparticles on the properties of fly ash blended cement, Nanomaterials 11 (2021) 1003.
[118] M. Tadic, D. Trpkov, L. Kopanja, S. Vojnovic, M. Panjan, Hydrothermal synthesis of hematite (α-Fe2O3) nanoparticle forms: synthesis conditions, structure, particle shape analysis, cytotoxicity and magnetic properties, J. Alloys Compd. 792 (2019) 599–609.
[119] Y. Wang, J. Schenk, J. Zhang, Z. Liu, J. Wang, L. Niu, et al., Novel sintering indexes to evaluate and correlate the crystal characteristics and compressive strength in magnetite pellets, Powder Technol. 362 (2020) 517–526.
[120] O. Gencel, W. Brostow, G. Martinez-Barrera, M.S. Gok, Mechanical properties of polymer concretes containing different amount of hematite or colemanite, Polimery 57 (2012) 276–283.
[121] S. Özen, M.Y. Durgun, V. Kobya, K. Karakuzu, A. Mardani-Aghabaglou, Effect of colemanite ore wastes utilization on fresh properties and compressive strength of cementitious systems, Arabian J. Sci. Eng. 47 (2022) 12873–12887.
[122] C. Kara, S. Kutuk, T. Kutuk-Sert, Improvement of the durability of concrete by substitution of raw ground colemanite, Case Stud. Constr. Mater. 19 (2023) e02393.
[123] G. Tochaikul, M. Mongkolsuk, P. Kobutree, S. Kawvised, P. Pairodsantikul, P. Wongsa, et al., Properties of cement Portland composite prepared with Barium sulfate and Bismuth oxide for radiation shielding, Radiat. Eff. Defect Solid (2023) 1–19.
[124] X. Cai, C. Liu, S. Zheng, H. Hu, Z. Tan, Analysis on the evolution characteristics of barite international trade pattern based on complex networks, Resour. Pol. 83 (2023) 103593.
[125] S.H.B. Clark, F.G. Poole, Z. Wang, Comparison of some sediment-hosted, stratiform barite deposits in China, the United States, and India, Ore Geol. Rev. 24 (2004) 85–101.
[126] S.K. Boamah, Comparative Analysis of Barite Production in Africa, 2019.
[127] I. Akkurt, H. Akyildirim, F. Karipçin, B. Mavi, Chemical corrosion on gamma-ray attenuation properties of barite concrete, J. Saudi Chem. Soc. 16 (2012) 199–202, https://doi.org/10.1016/j.jscs.2011.01.003.
[128] K. Janković, S. Stanković, D. Bojović, M. Stojanović, L. Antić, The influence of nano-silica and barite aggregate on properties of ultra high performance concrete, Construct. Build. Mater. 126 (2016) 147–156, https://doi.org/10.1016/j.conbuildmat.2016.09.026.
[129] S. Sharifi, R. Bagheri, S.P. Shirmardi, Comparison of shielding properties for ordinary, barite, serpentine and steel-magnetite concretes using MCNP-4C code and available experimental results, Ann. Nucl. Energy 53 (2013) 529–534, https://doi.org/10.1016/j.anucene.2012.09.015.
[130] F. Lo Monte, P.G. Gambarova, Thermo-mechanical behavior of baritic concrete exposed to high temperature, Cem. Concr. Compos. 53 (2014) 305–315, https://doi.org/10.1016/j.cemconcomp.2014.07.009.
[131] L. Tung-Chai, P. Chi-Sun, High temperatures properties of barite concrete with cathode ray tube funnel glass, Fire Mater. (2013), https://doi.org/10.1002/fam.
[132] E. Horszczaruk, P. Sikora, K. Cendrowski, E. Mijowska, The effect of elevated temperature on the properties of cement mortars containing nanosilica and heavyweight aggregates, Construct. Build. Mater. 137 (2017) 420–431, https://doi.org/10.1016/j.conbuildmat.2017.02.003.
[133] F. Demir, G. Budak, R. Sahin, A. Karabulut, M. Oltulu, K. Şerifoğlu, et al., Radiation transmission of heavyweight and normal-weight concretes containing colemanite for 6 MV and 18 MV X-rays using linear accelerator, Ann. Nucl. Energy 37 (2010) 339–344, https://doi.org/10.1016/j.anucene.2009.12.010.
[134] I. Akkurt, C. Basyigit, S. Kilincarslan, B. Mavi, The shielding of γ-rays by concretes produced with barite, Prog. Nucl. Energy 46 (2005) 1–11, https://doi.org/10.1016/j.pnucene.2004.09.015.

[135] I. Akkurt, H. Akyildirim, B. Mavi, S. Kilincarslan, C. Basyigit, Gamma-ray shielding properties of concrete including barite at different energies, Prog. Nucl. Energy 52 (2010) 620–623, https://doi.org/10.1016/j.pnucene.2010.04.006.
[136] I. Akkurt, C. Basyigit, S. Kilincarslan, B. Mavi, A. Akkurt, Radiation shielding of concretes containing different aggregates, Cem. Concr. Compos. 28 (2006) 153–157, https://doi.org/10.1016/j.cemconcomp.2005.09.006.
[137] I.I. Bashter, Calculation of radiation attenuation coefficients for shielding concretes, Ann. Nucl. Energy 24 (1997) 1389–1401, https://doi.org/10.1016/S0306-4549(97)00003-0.
[138] S.S. Obaid, D.K. Gaikwad, P.P. Pawar, Determination of gamma ray shielding parameters of rocks and concrete, Radiat. Phys. Chem. 144 (2018) 356–360, https://doi.org/10.1016/j.radphyschem.2017.09.022.
[139] I. Sosa, C. Thomas, J.A. Polanco, J. Setién, P. Tamayo, High performance self-compacting concrete with electric arc furnace slag aggregate and cupola slag powder, Appl. Sci. 10 (2020), https://doi.org/10.3390/app10030773.
[140] P. Tamayo, J. Pacheco, C. Thomas, J. de Brito, J. Rico, Mechanical and durability properties of concrete with coarse recycled aggregate produced with electric arc furnace slag concrete, Appl. Sci. 10 (2020), https://doi.org/10.3390/app10010216.
[141] M. Maslehuddin, A.A. Naqvi, M. Ibrahim, Z. Kalakada, Radiation shielding properties of concrete with electric arc furnace slag aggregates and steel shots, Ann. Nucl. Energy 53 (2013) 192–196, https://doi.org/10.1016/j.anucene.2012.09.006.
[142] A.G. Hassan, H. Elkady, A.S. Faried, M.A. Hassan, M.E. Allam, Evaluation of electric arc furnace slag high strength shielding concrete on exposure to gamma 662 KeV, Case Stud. Constr. Mater. 13 (2020), https://doi.org/10.1016/j.cscm.2020.e00416.
[143] S.I. Abu-Eishah, A.S. El-Dieb, M.S. Bedir, Performance of concrete mixtures made with electric arc furnace (EAF) steel slag aggregate produced in the Arabian Gulf region, Construct. Build. Mater. 34 (2012) 249–256, https://doi.org/10.1016/j.conbuildmat.2012.02.012.
[144] A. Santamaría, E. Rojí, M. Skaf, I. Marcos, J.J. González, The use of steelmaking slags and fly ash in structural mortars, Construct. Build. Mater. 106 (2016) 364–373, https://doi.org/10.1016/j.conbuildmat.2015.12.121.
[145] J.J. Chang, W. Yeih, T.J. Chung, R. Huang, Properties of pervious concrete made with electric arc furnace slag and alkali-activated slag cement, Construct. Build. Mater. 109 (2016) 34–40, https://doi.org/10.1016/j.conbuildmat.2016.01.049.
[146] C.A. Montenegro Neyra, Las Infecciones del Tracto Urinario Durante el Embarazo y su Relación con el Parto Pretérmino, Univ Cesar Vallejo 26 (2019) 1–55.
[147] A. Yadollahi, E. Nazemi, A. Zolfaghari, A.M. Ajorloo, Optimization of thermal neutron shield concrete mixture using artificial neural network, Nucl. Eng. Des. 305 (2016) 146–155, https://doi.org/10.1016/j.nucengdes.2016.05.012.
[148] L. Wadsö, C.P. Cooper-Jensen, P.M. Bentley, Assessing hydration disturbances from concrete aggregates with radiation shielding properties by isothermal calorimetry, Phys. Rev. Accel. Beams 20 (2017), https://doi.org/10.1103/PhysRevAccelBeams.20.043502.
[149] R. Adeli, S.P. Shirmardi, R. Bagheri, Theory and simulation investigation of low-energy neutron shielding for different boron compounds, J. Test. Eval. 45 (2017) 1570–1576, https://doi.org/10.1520/JTE20160060.
[150] D. Sariyer, R. Küçer, N. Küçer, Neutron shielding properties of concretes containing boron carbide and ferro boron, Procedia Soc. Behav. Sci. 195 (2015) 1752–1756.
[151] O. Gencel, W. Brostow, C. Ozel, M. Filiz, An investigation on the concrete properties containing colemanite, Int. J. Phys. Sci. 5 (2010) 216–225.
[152] A. Khajeali, A.R. Farajollahi, R. Khodadadi, Y. Kasesaz, A. Khalili, Role of gel dosimeters in boron neutron capture therapy, Appl. Radiat. Isot. 103 (2015) 72–81, https://doi.org/10.1016/j.apradiso.2015.05.017.
[153] S.E. Chidiac, M.G. El-Samrah, M.A. Reda, M.A.E. Abdel-Rahman, Mechanical and radiation shielding properties of concrete containing commercial boron carbide powder, Construct. Build. Mater. 313 (2021), https://doi.org/10.1016/j.conbuildmat.2021.125466.
[154] S. Ebrahimi, M.S. Heydari, H.R. Baharvandi, N. Ehsani, Effect of iron on the wetting, sintering ability, and the physical and mechanical properties of boron carbide composites: a review, Int. J. Refract. Met. Hard Mater. 57 (2016) 78–92, https://doi.org/10.1016/j.ijrmhm.2016.02.007.
[155] M.K. Moradllo, C.W. Chung, M.H. Keys, A. Choudhary, S.R. Reese, W.J. Weiss, Use of borosilicate glass powder in cementitious materials: pozzolanic reactivity and neutron shielding properties, Cem. Concr. Compos. 112 (2020), https://doi.org/10.1016/j.cemconcomp.2020.103640.
[156] U.K. Sevim, Colemanite ore waste concrete with low shrinkage and high split tensile strength, Mater Struct Constr 44 (2011) 187–193, https://doi.org/10.1617/s11527-010-9618-4.
[157] O. Gencel, Effect of elevated temperatures on mechanical properties of high-strength concrete containing varying proportions of hematite, Fire Mater. 36 (2012) 217–230, https://doi.org/10.1002/fam.1102.
[158] A.M. Ibrahim, A.R. Mohamed, A.M. El-Khatib, M.T. Alabsy, M. Elsalamawy, Effect of hematite and iron slag as aggregate replacement on thermal, mechanical, and gamma-radiation shielding properties of concrete, Construct. Build. Mater. 310 (2021) 125225, https://doi.org/10.1016/j.conbuildmat.2021.125225.
[159] O. Gencel, W. Brostow, C. Ozel, M. Filiz, Concretes containing hematite for use as shielding barriers, Medziagotyra 16 (2010) 249–256.
[160] I. Asadi, P. Shafigh, Z.F.B.A. Hassan, N.B. Mahyuddin, Thermal conductivity of concrete–A review, J. Build. Eng. 20 (2018) 81–93.
[161] Y. Grosu, A. Faik, I. Ortega-Fernández, B. D'Aguanno, Natural Magnetite for thermal energy storage: excellent thermophysical properties, reversible latent heat transition and controlled thermal conductivity, Sol. Energy Mater. Sol. Cells 161 (2017) 170–176.
[162] Y. Lv, Y. Qin, J. Wang, G. Li, P. Zhang, D. Liao, et al., Effect of incorporating hematite on the properties of ultra-high performance concrete including nuclear radiation resistance, Construct. Build. Mater. 327 (2022) 126950, https://doi.org/10.1016/j.conbuildmat.2022.126950.
[163] M.M. Tufekci, A. Gokce, Development of heavyweight high performance fiber reinforced cementitious composites (HPFRCC)–Part II: X-ray and gamma radiation shielding properties, Construct. Build. Mater. 163 (2018) 326–336.
[164] M.S. Selim, A. Elmarakbi, A.M. Azzam, M.A. Shenashen, A.M. EL-Saeed, S.A. El-Safty, Eco-friendly design of superhydrophobic nano-magnetite/silicone composites for marine foul-release paints, Prog. Org. Coating 116 (2018) 21–34, https://doi.org/10.1016/j.porgcoat.2017.12.008.
[165] D.I. Groves, N.M. Vielreicher, The Phalabowra (Palabora) carbonatite-hosted magnetite–copper sulfide deposit, South Africa: an end-member of the iron-oxide copper–gold–rare earth element deposit group? Miner. Deposits 36 (2001) 189–194.
[166] A.M. El-Khayatt, Radiation shielding of concretes containing different lime/silica ratios, Ann. Nucl. Energy 37 (2010) 991–995, https://doi.org/10.1016/j.anucene.2010.03.001.
[167] K. Gunoglu, İ. Akkurt, Radiation shielding properties of concrete containing magnetite, Prog. Nucl. Energy 137 (2021) 103776, https://doi.org/10.1016/j.pnucene.2021.103776.
[168] Y. Esen, Z.M. Doğan, Evaluation of physical and mechanical characteristics of siderite concrete to be used as heavy-weight concrete, Cem. Concr. Compos. 82 (2017) 117–127.
[169] A. Christogerou, T. Kavas, Y. Pontikes, S. Koyas, Y. Tabak, G.N. Angelopoulos, Use of boron wastes in the production of heavy clay ceramics, Ceram. Int. 35 (2009) 447–452, https://doi.org/10.1016/j.ceramint.2007.12.001.
[170] T.W. Davies, S. Çolak, R.M. Hooper, Boric acid production by the calcination and leaching of powdered colemanite, Powder Technol. 65 (1991) 433–440, https://doi.org/10.1016/0032-5910(91)80204-V.
[171] K. Okuno, H. Matsue, S. Miyata, Y. Kiyanagi, Neutron activation property of colemanite-peridotite concrete, Nucl. Sci. Eng. 173 (2013) 139–149, https://doi.org/10.13182/NSE12-15.
[172] M. Kinno, K.I. Kimura, T. Nakamura, Raw materials for low-activation concrete neutron shields, J. Nucl. Sci. Technol. 39 (2002) 1275–1280, https://doi.org/10.1080/18811248.2002.9715321.
[173] Y. Yarar, Activation characteristics of concrete shields containing colemanite, J. Nucl. Mater. 233–237 (1996) 1511–1515, https://doi.org/10.1016/S0022-3115(96)00324-8.
[174] H. Binici, O. Aksogan, A.H. Sevinc, A. Kucukonder, Mechanical and radioactivity shielding performances of mortars made with colemanite, barite, ground basaltic pumice and ground blast furnace slag, Construct. Build. Mater. 50 (2014) 177–183, https://doi.org/10.1016/j.conbuildmat.2013.09.033.
[175] K. Karimi-Shahri, L. Rafat-Motavalli, H. Miri-Hakimabad, Finding a suitable shield for mixed neutron and photon fields based on an Am-Be source, J. Radioanal. Nucl. Chem. 298 (2013) 33–39, https://doi.org/10.1007/s10967-012-2225-9.

[176] E. Erdogmus, Combined effect of waste colemanite and silica fume on properties of cement mortar, Sci. Eng. Compos. Mater. 21 (2014) 369–375, https://doi.org/10.1515/secm-2013-0041.
[177] M.E. Mahmoud, A.M. El-Khatib, M.S. Badawi, A.R. Rashad, R.M. El-Sharkawy, A.A. Thabet, Recycled high-density polyethylene plastics added with lead oxide nanoparticles as sustainable radiation shielding materials, J. Clean. Prod. 176 (2018) 276–287, https://doi.org/10.1016/j.jclepro.2017.12.100.
[178] M. Rashad, H.O. Tekin, H.M. Zakaly, M. Pyshkina, S.A.M. Issa, G. Susoy, Physical and nuclear shielding properties of newly synthesized magnesium oxide and zinc oxide nanoparticles, Nucl. Eng. Technol. 52 (2020) 2078–2084, https://doi.org/10.1016/j.net.2020.02.013.
[179] K. Verdipoor, A. Alemi, A. Mesbahi, Photon mass attenuation coefficients of a silicon resin loaded with WO3, PbO, and Bi2O3 Micro and Nano-particles for radiation shielding, Radiat. Phys. Chem. 147 (2018) 85–90, https://doi.org/10.1016/j.radphyschem.2018.02.017.
[180] A.M. Onaizi, G.F. Huseien, N.H.A.S. Lim, M. Amran, M. Samadi, Effect of nanomaterials inclusion on sustainability of cement-based concretes: a comprehensive review, Construct. Build. Mater. 306 (2021) 124850.
[181] N. Damla, U. Cevik, A.I. Kobya, A. Celik, N. Celik, R. Van Grieken, Radiation dose estimation and mass attenuation coefficients of cement samples used in Turkey, J. Hazard Mater. 176 (2010) 644–649, https://doi.org/10.1016/j.jhazmat.2009.11.080.
[182] J. Kim, D. Seo, B.C. Lee, Y.S. Seo, W.H. Miller, Nano-W dispersed gamma radiation shielding materials, Adv. Eng. Mater. 16 (2014) 1083–1089, https://doi.org/10.1002/adem.201400127.
[183] H.O. Tekin, M.I. Sayyed, S.A.M. Issa, Gamma radiation shielding properties of the hematite-serpentine concrete blended with WO3 and Bi2O3 micro and nano particles using MCNPX code, Radiat. Phys. Chem. 150 (2018) 95–100, https://doi.org/10.1016/j.radphyschem.2018.05.002.
[184] J. Qiao, X. Zhang, D. Xu, L. Kong, L. Lv, F. Yang, et al., Design and synthesis of TiO2/Co/carbon nanofibers with tunable and efficient electromagnetic absorption, Chem. Eng. J. 380 (2020), https://doi.org/10.1016/j.cej.2019.122591.
[185] H. Liang, J. Liu, Y. Zhang, L. Luo, H. Wu, Ultra-thin broccoli-like SCFs@TiO2 one-dimensional electromagnetic wave absorbing material, Composites, Part B 178 (2019), https://doi.org/10.1016/j.compositesb.2019.107507.
[186] H. Deng, X. Li, Q. Peng, X. Wang, J. Chen, Y. Li, Monodisperse magnetic single-crystal ferrite microspheres, Angew. Chem. Int. Ed. 44 (2005) 2782–2785, https://doi.org/10.1002/anie.200462551.
[187] D. Honecker, L. Fernández Barquín, P. Bender, Magnetic structure factor of correlated moments in small-angle neutron scattering, Phys. Rev. B 101 (2020), https://doi.org/10.1103/PhysRevB.101.134401.
[188] I. Vrdoljak, D. Varevac, I. Miličević, S. Čolak, Concrete-based composites with the potential for effective protection against electromagnetic radiation: a literature review, Construct. Build. Mater. 326 (2022), https://doi.org/10.1016/j.conbuildmat.2022.126919.
[189] C.H. Phan, M. Mariatti, Y.H. Koh, Electromagnetic interference shielding performance of epoxy composites filled with multiwalled carbon nanotubes/manganese zinc ferrite hybrid fillers, J. Magn. Magn Mater. 401 (2016) 472–478, https://doi.org/10.1016/j.jmmm.2015.10.067.
[190] P. Shahmohamadi, F. Soflaee, The combination of clay and nanotube carbon as an innovative and sustainable material, 2nd PALENC Conf 2 (2007) 959–963.
[191] M. Jung, Y soon Lee, S.G. Hong, J. Moon, Carbon nanotubes (CNTs) in ultra-high performance concrete (UHPC): dispersion, mechanical properties, and electromagnetic interference (EMI) shielding effectiveness (SE), Cement Concr. Res. 131 (2020), https://doi.org/10.1016/j.cemconres.2020.106017.
[192] M. Sharif, C.S. Ping, K.Y. Leong, Electromagnetic interference shielding performances of MWCNT in concrete composites, Solid State Phenom. 266 SSP (2017) 283–286, https://doi.org/10.4028/www.scientific.net/SSP.266.283.
[193] D. Micheli, R. Pastore, A. Vricella, R.B. Morles, M. Marchetti, A. Delfini, et al., Electromagnetic characterization and shielding effectiveness of concrete composite reinforced with carbon nanotubes in the mobile phones frequency band, Mater. Sci. Eng. B Solid-State Mater. Adv. Technol. 188 (2014) 119–129, https://doi.org/10.1016/j.mseb.2014.07.001.
[194] D. Micheli, M. Marchetti, R. Pastore, A. Vricella, G. Gradoni, F. Moglie, et al., Shielding effectiveness of carbon nanotube reinforced concrete composites by reverberation chamber measurements, Proc. 2015 Int. Conf. Electromagn. Adv. Appl. ICEAA (2015, 2015) 145–148, https://doi.org/10.1109/ICEAA.2015.7297092.
[195] D. Micheli, A. Vricella, R. Pastore, A. Delfini, R. Bueno Morles, M. Marchetti, et al., Electromagnetic properties of carbon nanotube reinforced concrete composites for frequency selective shielding structures, Construct. Build. Mater. 131 (2017) 267–277, https://doi.org/10.1016/j.conbuildmat.2016.11.078.
[196] N. Lee, S. Kim, G. Park, The effects of multi-walled carbon nanotubes and steel fibers on the AC impedance and electromagnetic shielding effectiveness of high-performance, fiber-reinforced cementitious composites, Materials 12 (2019), https://doi.org/10.3390/ma12213591.
[197] Y. Zhang, X.H. Wang, J.H. Luo, Research on absorbing property of cement-based material blending with nano-TiO2 and steel fibers, Adv. Mater. Res. 853 (2014) 207–211, https://doi.org/10.4028/www.scientific.net/AMR.853.207.
[198] J.M. Chiou, Q. Zheng, D.D.L. Chung, Electromagnetic interference shielding by carbon fibre reinforced cement, Composites 20 (1989) 379–381, https://doi.org/10.1016/0010-4361(89)90663-0.
[199] D.-Y. Yoo, M.-C. Kang, H.-J. Choi, W. Shin, S. Kim, Influence of chemically treated carbon fibers on the electromagnetic shielding of ultra-high-performance fiber-reinforced concrete, Arch. Civ. Mech. Eng. 20 (2020) 1–15.
[200] G. Park, S. Kim, G.-K. Park, N. Lee, Influence of carbon fiber on the electromagnetic shielding effectiveness of high-performance fiber-reinforced cementitious composites, J. Build. Eng. 35 (2021) 101982.
[201] T. Ichikawa, H. Koizumi, Possibility of radiation-induced degradation of concrete by alkali-silica reaction of aggregates, J. Nucl. Sci. Technol. 39 (2002) 880–884, https://doi.org/10.1080/18811248.2002.9715272.
[202] I. Maruyama, O. Kontani, S. Sawada, O. Sato, G. Igarashi, M. Takizawa, Evaluation of irradiation effects on concrete structure-background and preparation of neutron irradiation test, Am. Soc. Mech. Eng. Power Div. POWER 2 (2013), https://doi.org/10.1115/POWER2013-98114.
[203] K.G. Field, I. Remec, Y Le Pape, Radiation effects in concrete for nuclear power plants - Part I: quantification of radiation exposure and radiation effects, Nucl. Eng. Des. 282 (2015) 126–143, https://doi.org/10.1016/j.nucengdes.2014.10.003.
[204] A.F. Cohen, Low-temperature thermal conductivity in neutron irradiated vitreous silica, J. Appl. Phys. 29 (1958) 591–593.
[205] L. Hobbs, M.R. Pascucci, Radiolysis and defect structure in electron-irradiated alpha-quartz, J. Phys. Colloq. 41 (1979) 237–242.
[206] M.F. Kaplan, Concrete Radiation Shielding, 1989.
[207] B. Pomaro, V.A. Salomoni, F. Gramegna, G. Prete, C.E. Majorana, Radiation damage evaluation on concrete within a facility for selective production of exotic species (SPES project), Italy, J. Hazard Mater. 194 (2011) 169–177, https://doi.org/10.1016/j.jhazmat.2011.07.079.
[208] I. Maruyama, O. Kontani, M. Takizawa, S. Sawada, S. Ishikawa, J. Yasukouchi, et al., Development of soundness assessment procedure for concrete members affected by neutron and gamma-ray irradiation, J. Adv. Concr. Technol. 15 (2017) 440–523, https://doi.org/10.3151/jact.15.440.
[209] J.F. Sommers, Gamma radiation damage of structural concrete immersed in water, Health Phys. 16 (1969) 503–508, https://doi.org/10.1097/00004032-196904000-00011.
[210] P. Soo, L.M. Milian, The effect of gamma radiation on the strength of Portland cement mortars, J. Mater. Sci. Lett. 20 (2001) 1345–1348, https://doi.org/10.1023/A:1010971122496.
[211] F. Vodák, K. Trtík, V. Sopko, O. Kapičková, P. Demo, Effect of γ-irradiation on strength of concrete for nuclear-safety structures, Cement Concr. Res. 35 (2005) 1447–1451, https://doi.org/10.1016/j.cemconres.2004.10.016.
[212] P. Sikora, M. Chougan, K. Cuevas, M. Liebscher, V. Mechtcherine, S.H. Ghaffar, et al., The effects of nano- and micro-sized additives on 3D printable cementitious and alkali-activated composites: a review, Appl. Nanosci. (2021), https://doi.org/10.1007/s13204-021-01738-2.
[213] L. Chang, Y. Zhang, Y. Liu, J. Fang, W. Luan, X. Yang, et al., Preparation and characterization of tungsten/epoxy composites for γ-rays radiation shielding, Nucl. Instrum. Methods Phys. Res. Sect. B Beam Interact. Mater. Atoms 356–357 (2015) 88–93, https://doi.org/10.1016/j.nimb.2015.04.062.
[214] I. Maruyama, S. Ishikawa, J. Yasukouchi, S. Sawada, R. Kurihara, M. Takizawa, et al., Impact of gamma-ray irradiation on hardened white Portland cement pastes exposed to atmosphere, Cement Concr. Res. 108 (2018) 59–71, https://doi.org/10.1016/j.cemconres.2018.03.005.
[215] Y. Reches, Nanoparticles as concrete additives: review and perspectives, Construct. Build. Mater. 175 (2018) 483–495, https://doi.org/10.1016/j.conbuildmat.2018.04.214.
[216] Y. Reches, A multi-scale review of the effects of gamma radiation on concrete, Results Mater 2 (2019) 100039, https://doi.org/10.1016/j.rinma.2019.100039.

[217] S. Yousef, M. AlNassar, B. Naoom, S. Alhajali, M.H. Kharita, Heat effect on the shielding and strength properties of some local concretes, Prog. Nucl. Energy 50 (2008) 22–26.
[218] C. Basyigit, I. Akkurt, R. Altindag, S. Kilincarslan, A. Akkurt, B. Mavi, et al., The effect of freezing–thawing (F–T) cycles on the radiation shielding properties of concretes, Build. Environ. 41 (2006) 1070–1073.
[219] H. Shang, Y. Song, J. Ou, Behavior of air-entrained concrete after freeze-thaw cycles, Acta Mech. Solida Sin. 22 (2009) 261–266.
[220] N. Tsoulfanidis, Computational methods in reactor shielding, Nucl. Technol. 64 (1984) 102, https://doi.org/10.13182/nt84-a33331.
[221] M. Hassanzadeh, S.M. Sadat Kiai, Calculation of photon attenuation coefficient and dose rate in concrete with the addition of SiO2 and MnFe2O4 nanoparticles using MCNPX code and comparison with experimental results, Nucl. Sci. Tech. 29 (2018), https://doi.org/10.1007/s41365-018-0493-y.
[222] A.E.-S. Abdo, Calculation of the cross-sections for fast neutrons and gamma-rays in concrete shields, Ann. Nucl. Energy 29 (2002) 1977–1988.
[223] M. Mutlutürk, R. Altindag, G. Türk, A decay function model for the integrity loss of rock when subjected to recurrent cycles of freezing–thawing and heating–cooling, Int. J. Rock Mech. Min. Sci. 41 (2004) 237–244.
[224] R. Altindag, I.S. Alyildiz, T. Onargan, Mechanical property degradation of ignimbrite subjected to recurrent freeze–thaw cycles, Int. J. Rock Mech. Min. Sci. 41 (2004) 1023–1028.
[225] R.P. Khatri, V. Sirivivatnanon, J.L. Yang, Role of permeability in sulphate attack, Cement Concr. Res. 27 (1997) 1179–1189.
[226] K. Wu, W. Kang, L. Xu, D. Sun, F. Wang, G. De Schutter, Damage evolution of blended cement concrete under sodium sulfate attack in relation to ITZ volume content, Construct. Build. Mater. 190 (2018) 452–465.
[227] H. Binici, O. Aksogan, A.H. Sevinc, E. Cinpolat, Mechanical and radioactivity shielding performances of mortars made with cement, sand and egg shells, Construct. Build. Mater. 93 (2015) 1145–1150.
[228] A. Łowińska-Kluge, P. Piszora, Effect of gamma irradiation on cement composites observed with XRD and SEM methods in the range of radiation dose 0-1409 MGy, Acta Phys Pol A 114 (2008) 399–411.
[229] Y. Le Pape, K.G. Field, I. Remec, Radiation effects in concrete for nuclear power plants, Part II: perspective from micromechanical modeling, Nucl. Eng. Des. 282 (2015) 144–157, https://doi.org/10.1016/j.nucengdes.2014.10.014.
[230] A. Attar, B. Gencturk, M. Hanifehzadeh, K. Willam, Accelerated aging of concrete dry cask storage systems for nuclear waste, J. Adv. Concr. Technol. 14 (2016) 299–310, https://doi.org/10.3151/jact.14.299.
[231] F. Sanchez, Development of nano-modified concrete for next generation of storage systems, Sci/Tech Rep Intellect Prop (2018), https://doi.org/10.2172/1469196.
[232] D.L. Fillmore, Literature Review of the Effects of Radiation and Temperature on the Aging of Concrete - Prepared for the Central Research Institute of Electric Power Institute - INEEL/EXT-04-02319, 2004, pp. 1–16.
[233] Z. Shen, H. Zhou, A. Brooks, D. Hanna, Evolution of elastic and thermal properties of cementitious composites containing micro-size lightweight fillers after exposure to elevated temperature, Cem. Concr. Compos. 118 (2021), https://doi.org/10.1016/j.cemconcomp.2021.103931.
[234] Y. Le Pape, A. Giorla, J. Sanahuja, Combined effects of temperature and irradiation on concrete damage, J. Adv. Concr. Technol. 14 (2016) 70–86, https://doi.org/10.3151/jact.14.70.
[235] J. Lee, Y. Xi, K. Willam, Y. Jung, A multiscale model for modulus of elasticity of concrete at high temperatures, Cement Concr. Res. 39 (2009) 754–762.
[236] K.D. Hertz, Concrete strength for fire safety design, Mag. Concr. Res. 57 (2005) 445–453.
[237] A.G. Pérez-Luna, A.L. Martínez-Hernández, G. Martínez-Barrera, C. Velasco-Santos, Nanoreinforced concrete: effect of gamma-irradiated SiO2 nanoparticles, Adv. Mater. Lett. 7 (2016) 156–162, https://doi.org/10.5185/amlett.2016.6145.
[238] M.F. Kaplan, Concrete Radiation Shielding : Nuclear Physics, Concrete Properties, Design and Construction, Longman Scientific & Technical, 1989.
[239] Y. Reches, K. Thomson, M. Helbing, D.S. Kosson, F. Sanchez, Agglomeration and reactivity of nanoparticles of SiO2, TiO2, Al2O3, Fe2O3, and clays in cement pastes and effects on compressive strength at ambient and elevated temperatures, Construct. Build. Mater. 167 (2018) 860–873, https://doi.org/10.1016/j.conbuildmat.2018.02.032.
[240] T. Ichikawa, T. Kimura, Effect of nuclear radiation on alkali-silica reaction of concrete, J. Nucl. Sci. Technol. 44 (2007) 1281–1284, https://doi.org/10.3327/jnst.44.1281.
[241] Q. Xu, J. Stark, Early hydration of ordinary Portland cement with an alkaline shotcrete accelerator, Adv. Cement Res. 17 (2005) 1–8, https://doi.org/10.1680/adcr.2005.17.1.1.
[242] E.R. Elsharkawy Mms, Effect of gamma ray energies and addition of nano-SiO2 to cement on the mechanical properties and mass attenuation coefficient, IOSR J. Mech. Civ. Eng. 13 (2013) 17–22.
[243] B. Fournier, M.A. Bérubé, Alkali-aggregate reaction in concrete: a review of basic concepts and engineering implications, Can. J. Civ. Eng. 27 (2000) 167–191, https://doi.org/10.1139/l99-072.
[244] V.E. Saouma, M.A. Hariri-Ardebili, A proposed aging management program for alkali silica reactions in a nuclear power plant, Nucl. Eng. Des. 277 (2014) 248–264, https://doi.org/10.1016/j.nucengdes.2014.06.012.
[245] L. Struble, S. Diamond, Unstable swelling behaviour of alkali silica gels, Cement Concr. Res. 11 (1981) 611–617, https://doi.org/10.1016/0008-8846(81)90091-0.
[246] L.P. Elleuch, F. Dubois, J. Rappeneau, Effects of Neutron Radiation on Special Concretes and Their Components, SP-034, Am. Concr. Institute, ACI Spec. Publ., 1972, pp. 1071–1108.
[247] J.T. Busby, P.G. Oberson, C.E. Carpenter, M. Srinivasan, Expanded materials degradation assessment (EMDA) volume 5 : aging of cables and cable systems, US NRC Rep 5 (2013).